MATERNAL *UBE3A* IS REQUIRED FOR NEUROTYPICAL MOTIVATIONAL DRIVE AND GABA CO-RELEASE

Janet Berrios

A dissertation submitted to the faculty at the University of North Carolina at Chapel Hill in partial fulfillment of the requirements for the degree of Doctor of Philosophy in the Neurobiology Curriculum in the School of Medicine.

Chapel Hill
2015

Approved by:

Thomas Kash

Paul Manis

Benjamin Philpot

Donita Robinson

Garret Stuber

ABSTRACT

Janet Berrios: Maternal UBE3A is required for neurotypical motivational drive and GABA co-release
(Under the direction of Benjamin D. Philpot)

Dopaminergic projections from the ventral tegmental area (VTA) to the nucleus accumbens (NAc) are known to be critical players in motivated, reward-seeking behaviors and are involved in learning processes during positive-reinforcement. These neurons co-release several neurotransmitters in the NAc, however; their differential role in motivation and positive-reinforcement is unknown. Angelman syndrome (AS) is a neurodevelopmental disorder caused by the deletion or mutation of the E3-ubiquitin ligase, *Ube3a*. *Ube3a* is monoallelically expressed from the maternal allele and is paternally imprinted in a tissue specific manner. Mouse models of AS have been shown to have dopaminergic related phenotypes such as ataxia and decreased brain stimulation reward (BSR) threshold. This decrease in BSR is thought to be mediated, in part, by an increase in dopamine release within the NAc as evidenced within AS model mice using electrically mediated BSR. Because of this increase in dopamine release within the NAc, we hypothesized that VTA-to-NAc projections were hyperexcitable leading to dopaminergic dysregulation. We used a combinatorial approach of *in vivo* and *in vitro* optogenetics to determine if dopaminergic projections from the VTA-to-NAc were specifically driving an increase in motivational drive and dopamine release.

Using circuit-specific manipulations, we found that there was not a change in dopamine release in AS model mice, but that there was a significant increase in motivational drive to self-stimulate these VTA axons in the NAc using a 1:1 fixed-ratio operant task. Next, we determined if *Ube3a* is required for neurotypical motivational drive using a novel conditional deletion mouse model (*Ube3a*$^{FLOX/p+}$) in which *Ube3a* was deleted from tyrosine hydroxylase (TH) positive neurons. We found that upon conditional *Ube3a* deletion, dopamine release remained at similar levels to wildtype mice however, motivational drive was significantly increased to a similar degree as in AS model mice.

We then hypothesized that the change in motivational drive was mediated by GABA or glutamate co-release. Previously, an inhibitory imbalance phenotype was found in AS model mice in which they have a decrease in inhibitory drive. We used *in vitro* optogenetics in conjunction with electrophysiology to determine if GABA and glutamate co-release was affected when *Ube3a* is specifically ablated in TH-positive neurons. We found that GABA co-release was severely compromised when *Ube3a* is ablated but glutamate co-release was unaffected. We also found that these phenotypes can be rescued upon exogenous expression of VGAT, a vesicular GABA transporter.

Here, we suggest a novel role for GABA co-release in VTA-to-NAc terminals in a mouse model for Angelman syndrome. Using *in vivo* and *in vitro* optogenetic combinatorial approaches, our findings suggest a new utility for the E3-ubiqutin ligase, *Ube3a,* in inhibitory transmission from dopaminergic fibers in the ventral striatum.

To my Dad, who taught me that anything is possible and gave me the world.

ACKNOWLEDGEMENTS

First, I would like to thank my advisor, Ben Philpot. Ben has encouraged me to always follow my instinct, good or bad. Without such a supportive advisor, I would not have stumbled upon such a great project that has solidified my love for science. It has not been an easy road and I thank Ben for making every day coming into lab exciting and providing a great working environment that was not only intellectually enriching but also, a fun place to be that made work feel less like work. Ben has always encouraged me to persevere and follow my gut, and without this support I would not have believed that I was capable of achieving what I have done.

Second, I would like to thank Garret Stuber. He welcomed me into his lab and he, and his lab members, made me feel welcomed and a part of their team. They have taught me an incredible amount and the knowledge they shared was invaluable. Without you all, the days would have been much longer, surgeries much less fun, and the experiments near impossible. Thank you Pranish Kantak, Alice Stamatakis Jennings, Joshua Jennings, Dennis Sparta, Shanna Resendez, Jim Otis, Zoe McElligott, and Jenna McHenry.

I would like to thank my lab mates that have been integral to my scientific development and my coffee addiction: Rylan Larsen, Matthew Judson, Mike Wallace, Thorfinn Riday, Adam Roberts, Jaya Miriyala, Megumi Aita, Kelly Jones, Hsien-Sung Huang, Courtney Thaxton, Angie Mabb, Bram Kuijer, Hanji Han, Mike Sidorov, and Sally Kim.

In addition, I would like to thank my dissertation committee members Tom Kash, Donita Robinson, Garret Stuber, and Paul Manis. I always looked forward to committee meetings as they have always been extremely helpful and has guided my project in the best direction. I am so appreciative and thankful to have such a supportive and constructive committee.

I would also like to thank my family: Dad, Steve, Hannah and Mom for supporting me over the years. Lastly, I would like to thank Mike Wallace I couldn't have done this without you and am so glad that you were with me every step of the way.

TABLE OF CONTENTS

LIST OF FIGURES

LIST OF ABBREVIATIONS

AMPA – α-amino-3-hyroxy-5-methyl-4-isoxazolepropionic acid

AMPAR – AMPA receptor

AP – Action Potential

AS – Angelman Syndrome

BLA – Basolateral Amygdala

BSR – Brain Stimulation Reward

CeA – Central Amygdala

ChR2 – Channel Rhodopsin-2

C_m – Capcitance

CPP – Conditioned Place Preference

DA – Dopamine

EYFP – Enhanced Yellow Fluorescent Protein

FSCV – Fast Scan Cyclic Voltammetry

GABA – gamma-aminobutyric acid

HPV – Human Papilloma Virus

Hz – Hertz

ICSS – Intracranial self-stimulation

i.p. – intraperitoneal

L-DOPA – levodopa

LTP – Long Term Potentiation

MeCP2 – methyl CpG binding domain 2

mEPSC/IPSC – miniature Excitatory/Inhibitory Post-syanptic currents

ms – milliseconds

MSN – Medium Spiny Neuron

NAc – Nucleus Accumbens

NMDA – N-methyl-D-aspartic acid

NMDAR – NMDA receptor

oIPSC/oEPSC – optical E/IPSC

PFC – Prefrontal Cortex

PPR – Paired-Pulse Ratio

RTPP- real-time place preference

sEPSC/IPSC – spontaneous Excitatory/Inhibitory post-synaptic current

SNc – Substantia Nigra pars compacta

TDE – Temporal Difference Error

TH – Tyrosine Hydroxylase

TH^+ - TH positive

VGAT – vesicular GABA transporter

VMAT2 – vesicular monoamine transporter – 2

VTA – Ventral Tegmental Area

WT – wildtype

YFP – Yellow Fluorescent Protein

CHAPTER 1

INTRODUCTION

The aim of this dissertation project was to address the hypotheses that the gene, *Ube3a*, (i) is a potential molecular regulator of motivational drive, (ii) causes hyperexcitability in reward circuitry within *Ube3a* deficient mice, and (iii) is not directly involved in dopamine release from ventral tegmental area projections to the nucleus accumbens. To address these hypotheses I employed a combinatorial approach of *in vivo* and *in vitro* optogenetics along with *in vitro* electrophysiology, *in vitro* fast-scan cyclic voltammetry, and operant conditioning paradigms.

As an introduction to this subject matter, subsections have been organized to provide a review of the applicable topics that include: (i) Angelman syndrome and mouse models of Angelman syndrome including the pathogenesis and phenotypes shared between mice and humans, (ii) neural circuits involved in reward-seeking and motivational drive including neurotransmission that has been defined as motivational regulators, and (iii) dopaminergic phenotypes that have been identified in other neurodevelopmental mouse models.

1.1 Angelman Syndrome: identification and known pathogenic molecular players

1.1.1 The discovery and early characterization of Angelman syndrome

Angelman syndrome (AS) was first described by Harry Angelman in 1965 in which he identified four key features in addition to severe developmental delay: flat occiput, tremulous movement, protruding tongues, and frequent laughter (Angelman, 1965). Because of these core features, he first described AS as "happy puppet syndrome." Principal features associated with AS have now been expanded and include an exhaustive list of associated phenotypes including (but not limited to): severe developmental delay, ataxia, frequent laughter, lack of speech, seizures, abnormal EEG, abnormal sleep-wake cycles, and tremors in adulthood (Williams et al., 2006).

1.1.2 Genetic causes of AS

AS has a penetrance of 1 in 12,000 and is a single gene disorder associated with the 15q11-13 chromosome that was first identified in 1987 (Clayton-Smith, 2003; Mabb et al., 2011; Williams et al., 2006). 15q11-13 (*UBE3A*) is known to be genetically imprinted, or silenced, on the paternal allele by a region known as an imprinting center. Genetic mutations and deletions associated with AS have been categorized into four different groups. These groups range from (i) de novo mutations, (ii) imprinting deficits leading to mutations or deletions, (iii) mosaic

imprinting deficits, and (iv) *Ube3a* mutation or deletion, a gene that is encoded by 15q11-13 (Clayton Smith and Laan., 2003).

1.1.3 The pathogenesis of AS by a single gene, *Ube3a*

UBE3A is a HECT (Homologous to E6-AP Carboxyl Terminus)-containing E3 ubiquitin ligase that is encoded by the 15q11-13 chromosome. UBE3A was first identified as E6-Associated Protein (E6-AP) as a regulator of p53 protein expression in HeLa cells, assigning it an oncogenic role in human papilloma virus (HPV) (Talis et al., 1998). E6, along with E6-AP (or UBE3A), transfers ubiquitin to the substrate, p53, and then targets this protein for proteasomal degradation. This role for UBE3A, within heterologous cell lines, provided some mechanistic insight into the pathogenesis of AS which will be further described in section **1.1.4**.

The chromosomal region containing the gene *Ube3a* (15q11-13) was a known "hot-spot" for genomic imprinting or, silencing (Mabb et al., 2011; Matsuura et al., 1997; Nicholls and Knepper, 2001). This epigenetic phenomenon of imprinting results in alleles that are either paternally or maternally expressed making parent-of-origin inheritance of each allele critical. The paternal allele of *Ube3a* is regulated by differential methylation of a particular imprinting center -- the Prader-Willi Syndrome Imprinting Center (PWS-IC) -- that is upstream of the *Snurf* and *Snrpn* promoter regions (Landers et. al., 2005). The result of this differential methylation on the paternal allele is the transcription of the *Ube3a-ATS* (Antisense) that encodes for an RNA antisense transcript that silences the transcription of *Ube3a* from the paternal allele in *cis* (Landers et al., 2005; Mabb et al., 2011; Matsuura et

al., 1997). The imprinting of the paternal allele renders the maternal *Ube3a* allele vulnerable to mutations that could result in a loss-of-function or dysregulation of UBE3A protein. Intriguingly, this imprinting is conserved in mice as in humans lending to the feasibility of making mouse models mimicking the human heredity of *Ube3a*. Using a mouse model in which the yellow-fluorescent protein (YFP) is knocked into the *Ube3a* locus (*Ube3a*^{YFP}) it was discovered that *Ube3a* imprinting only occurs within post-mitotic neurons in the brain but is biallecially expressed within glia leading to cell type-specific expression of UBE3A within the brain (Dindot et al., 2008).

1.1.4 Neuronal phenotypes and proposed substrates of UBE3A

The AS field, in regards to described neuronal phenotypes, began with the engineering of an AS model mouse by Yong-hui Jiang that contained a targeted deletion at exon 2 (Jiang et al., 1998). This targeted disruption of *Ube3a* resulted in a null allele. Since maternal *Ube3a* is the allele that is expressed in neural tissue, it is of utmost importance to note parent-of-origin inheritance for the null allele. Therefore, all AS model mice are maternally deficient for *Ube3a* while the paternal allele remains intact. Because of the paternal imprinting, this renders the animal *null* for all neuronal UBE3A expression and AS model mice are denoted as: *Ube3a*$^{m-/p+}$.

The first phenotypes described within *Ube3a*$^{m-/p+}$ involved motor dysfunction, long-term potentiation (LTP) deficits, and upregulation of p53, a previously identified UBE3A substrate (Jiang et al., 1998). *Ube3a*-deficient mice were engineered by targeting exon 2 which deletes a portion of the N-terminal amino acids that

inactivates UBE3A protein. This seminal paper and novel mouse line spawned a new opportunity for neuroscientists to elucidate circuit deficits in a rare neurodevelopmental disorder. Neuronal phenotypes that have been described using this mouse line include (but are not limited to): decreased dendritic spine number and altered morphology (Dindot et al., 2008; Sato and Stryker, 2010; Yashiro et al., 2009), experience dependent plasticity deficits (Sato and Stryker, 2010; Yashiro et al., 2009), altered intrinsic membrane properties (Kaphzan et al., 2011), loss of inhibitory drive correlated to an increase in clathrin coated vesicles (Wallace et al., 2012), decreased locomotion (Huang et al., 2013; Riday et al., 2012), aberrant dopamine release (Riday et al., 2012), and dysregulation in circadian rhythm (Shi et al., 2015).

While a rich literature describing circuit and synaptic deficits within AS model mice has matured, there is still little information on potential substrates of UBE3A that leads to the development of these observed neuronal phenotypes. As previously mentioned, UBE3A was first identified as E6-Associated Protein in that it required an oncogenic cofactor (E6) to degrade p53. Because UBE3A is an E3-ubiquitin ligase, substrate identification has centered on identifying potential neuronal substrates by assessing correlated protein upregulation (Mabb et al., 2011). Neuronal substrates that have been identified have done so by using co-immunoprecipitations and differ based not only on cellular localization but also anatomically. The proposed UBE3A substrates are: p53, p27, Pbl, α-synuclein, Arc, Ephexin5, and GAT1 (Egawa et al., 2012; Mabb et al., 2011).

Interactions within the proteomic pathway are fairly quick (within minutes) and are composed of weak thioester covalent bonds (Cooper et al., 2004; Martinez-Noel et al., 2012). In addition, there are five subtypes of three different UBE3A isoforms, that differ within the N-terminus, leading to additional difficulty in identifying neuronal specific roles in anatomically distinct regions (Yamamoto et al., 1997). Because of the mechanism of action, the ubiquitin proteolysis pathway is, in itself, transient in that these complexes will be degraded within the proteasome. Biochemical analyses of complexes have therefore, been performed under conditions inhibiting the proteasome with MG132 (Cooper et al., 2004; Martinez-Noel et al., 2012; Yamamoto et al., 1997). These factors as a whole have, therefore, made the identification of a true neuronal-specific substrate difficult.

1.1.5 Dopaminergic phenotypes correlated with *Ube3a* loss

There are phenotypes present within AS patients that can be ascribed to dopaminergic dysfunction. These symptoms include ataxia and tremors that have been characterized as early-onset Parkinson's (Harbord, 2001; Riday et al., 2012). The presence of these symptoms have led to the hypothesis that dopaminergic dependent circuits are affected in AS patients and have led to the use of levodopa (L-DOPA) in clinical trials (Harbord, 2001); Tan W-H, *in progress*). While the use of L-DOPA in two elderly AS patients ameliorated tremors, it remained unclear as to how these symptoms arose (Harbord, 2001). In 2010, the Jana group suggested that the loss of *Ube3a* resulted in a loss of TH positive (TH^+) neurons in the substantia nigra compacta (SNc) leading to the motor phenotypes observed in AS model mice

(Mulherkar and Jana, 2010). However, this work does not take into account that the loss of TH^+ neurons does not necessarily coincide with a decrease in dopamine (DA) release or directly relate to behavioral phenotypes. In *drosophila,* it was identified that UBE3A associates with GTP cyclohydrolase the rate limiting factor in monoamine synthesis (Ferdousy et al., 2011). This work was further expanded upon in AS model mice by using microdialysis to measure the concentration of DA, serotonin, and norepinephrine within the striatum, midbrain and frontal cortex (Farook et al., 2012). Using this technique, an increase in catecholaminergic and serotoninergic concentration were found, however, microdialysis is only sufficient to measure extracellular concentration averaged across several minutes and does not take into account release mechanisms that occurs on a millisecond timescale.

The proposed dopaminergic phenotypes had only been correlated with changes in dopamine release and have not been shown to have a causal relationship. In addition, these were attributed to a *decrease* in release. In 2012, Riday et. al. used a combinatorial approach of behavior, *in vivo* fast-scan cyclic voltammetry, and biochemistry to assess dopamine content and release in AS model mice using a behavioral paradigm known to be dopamine dependent. Fast-scan cyclic voltammetry (FSCV) is the highest resolution method currently available to detect dopamine release *in vivo* and *in vitro* (Jones et al., 1996; Robinson et al., 2003) and can be used to detect changes in DA release with nanomolar precision in a subsecond timescale. Using *in vivo* FSCV, an opposing dysregulation in DA dynamics was found within AS model mice. Within the nigrostriatal pathway (SNc-to-dorsal striatum), voltammetric recordings revealed that there was a decrease in

electrically-evoked DA release in *Ube3a*-deficient mice and an increase within the mesolimbic pathway (VTA-to-NAc). This evidence corroborates previous publications suggesting that there is a decrease in DA within AS model mice that leads to motor deficits however, it was unknown how an increase would affect behaviors associated with the mesolimbic pathway. Interestingly, Riday and colleagues also validated that there was not a difference in the number of TH^+ neurons or dopamine tissue content in AS model mice when compared to controls which is in contrast to the previously described increase in catecholaminergic concentration (Farook et al., 2012; Mulherkar and Jana, 2010; Riday et al., 2012).

Intracranial self-stimulation (ICSS) is behavior paradigm that has been classically used to determine reward-threshold via electrical stimulation and is often referred to as brain stimulation reward (BSR) (Olds and Milner, 1954). This method of stimulation causes DA release and is essential to elicit synthetic "rewarding" behaviors. Accumbal DA release is associated with the euphoric effects associated with drugs of abuse (e.g. opioids, cocaine) as well as food and copulation (Fields and Margolis, 2015; Wise and Rompre, 1989). By placing a stimulating electrode within the medial forebrain bundle (MFB), this ICSS paradigm was used in AS model mice to test the hypothesis if the increase in electrically-evoked DA release found with FSCV resulted in an expected behavioral consequence. Indeed, *Ube3a*$^{m-/p+}$ mice had a lower threshold to maintain the BSR response and responded more over time, consistent with the increase in DA release within the NAc. These results are intriguing and represent the first direct evidence for a change in DA release within AS model mice that has a direct behavioral consequence. However, there is one

caveat that should be considered. The stimulating electrode used for both the ICSS paradigm and FSCV was placed within the MFB. The MFB contains axons that are heterogeneous and do not only project to the VTA but to other structures that will result in DA release within the NAc (Tsai et al., 2009). Therefore, observed changes in DA release using MFB stimulation are not necessarily due to DAergic neuron-specific excitation but may occur through additional circuit mechanisms.

1.2 Circuitry underlying reward-seeking and motivation

1.2.1 The identification of "pleasure centers" and dopamine as a rewarding neuromodulator

Neural circuits responsible for regulating motivation are necessary for survival. An animal must identify what behaviors should be repeated in order to gain access to pleasurable "rewards" such as sex, food, and social interaction. Olds and Milner (1954) hypothesized that there are "pleasure centers" of the brain and used BSR in various brain regions to assay which areas supported self-stimulation in mice. Their research identified a circuit responsible for "reward-seeking" by identifying anatomical regions responsible for the learning process that lead to positive-reinforcement which is, in part, mediated by dopamine (Robinson and Berridge, 1993; Schultz, 1998; Wise, 1978). The effect of dopamine as a reinforcing neuromodulator was first identified by lesioning selective anatomical regions in parallel. The use of BSR and the application of drugs of abuse, such as cocaine

(Schultz, 1998), helped in the identification of DA as a rewarding neuromodulator. The mesolimbic pathway, which is composed of projections from the VTA to the NAc, is the most well defined circuit involved in reward-seeking/motivational behavior.

1.2.2 The VTA: cell types, projections, and electrophysiological properties

The VTA, along with the SNc, is a major source of DA to the cortex and a majority of subcortical regions (Bjorklund and Dunnett, 2007; Bromberg-Martin et al., 2010). Neurons in the VTA are heterogeneous in cell types; most neurons are dopaminergic (~70%), and there are also GABAergic (~30%) interneurons, and a small percentage of glutamatergic neurons (~2%) (Nair-Roberts et al., 2008; Walsh and Han, 2014; Yamaguchi et al., 2007). The VTA sends a majority of its dopaminergic projections to the NAc but it is important to note that the VTA also sends dopaminergic projections to the prefrontal cortex (PFC), central amygdala (CeA), basolateral amygdala (BLA), and hippocampus (Russo and Nestler, 2013; Walsh and Han, 2014). In addition to the cell type heterogeneity within the VTA, dopaminergic neurons are now known to release several neurotransmitters in addition to dopamine, including GABA and glutamate (Stuber et al., 2010; Tritsch et al., 2012).

Dopaminergic neurons fire in two distinct patterns that have been characterized as tonic and phasic firing rates which differ in frequency. Tonic firing rates are low in frequency (1-5 Hz) and are maintained at a steady baseline level

which results in a basal level of available dopamine in target structures that is required for neurotransmission in those terminal fields (Bromberg-Martin et al., 2010; Grace, 1991; Grace et al., 2007; Grace and Onn, 1989; Lammel et al., 2008; Schultz, 2007; Tsai et al., 2009; Yim and Mogenson, 1980). Phasic firing rates are increased to >15 Hz and are triggered by external stimuli that signal the presence of reward and cause a large increase in DA concentration in downstream targets (Schultz, 1998; Tsai et al., 2009).

Identifying dopaminergic neurons within the VTA was previously simplified by looking at two distinct electrophysiological properties: the presence of an I_h (hyperpolarization-activated cyclic nucleotide-gated) current and intrinsic membrane properties that were first described within the SNc (Margolis et al., 2006). Because the SNc is adjacent to the VTA, and the neuronal composition is fairly homogenous (~90% dopaminergic) an assumption was made that the electrophysiological properties defined for TH^+ neurons within the SNc would apply to those in the VTA. However, Margolis et. al. determined that selecting for neurons in this fashion, within the VTA, results in inaccurate selection of DA containing neurons. Past hypotheses proposed that selecting for neurons with the presence of a pronounced I_h current is indicative of dopamine content. In contrast, thorough electrophysiological and molecular characterizations have shown that those cells with larger I_h currents are likely TH-negative and that the size of the current differs based on the downstream targets of those TH^+ projections (Ford et al., 2006; Margolis et al., 2006). In addition intrinsic membrane properties, action potential (AP) threshold, AP peak, AP width, soma size, or anatomical location does not provide any distinguishing parameters

between TH^+ and TH-negative cells (Margolis et al., 2006). Another characteristic of VTA dopaminergic neurons that increases the difficulty of accurately identifying them is that their electrophysiological properties will differ depending on where they send projections to (Lammel et al., 2008; Lammel et al., 2011; Lammel et al., 2014).

The challenge in identifying dopaminergic neurons within the VTA comes in the heterogeneity of responses. DA neurons that are within the medial VTA project to the mPFC, BLA, and NAc (core and shell). These neurons have little to no I_h, fire APs at high frequencies averaging 20-30 Hz, have broad action potentials and small after hyperpolarization, and have synapses with a high AMPAR/NMDAR conductance ratio (~0.6) (Lammel et al., 2014). DA neurons that have been shown to project to the NAc lateral shell are within the lateral VTA and have characteristic electrophysiological properties that were initially defined as: prominent I_h, AP firing frequencies up to 10 Hz, short AP half-width with large after hyperpolarizations and a low AMPA/NMDA ratio (~0.4) (Lammel et al., 2014). Because of the heterogeneity present in DA neurons within the VTA, there are several tools that have become necessary when selecting DA neurons for electrophysiology. These tools include *post-hoc* immunohistochemistry, RetroBeads (LumaFluor), fluorescently labeled cholera toxin, fluorescently coupled transgenic lines (e.g. TH-EGFP), and CRE dependent reporters (e.g. Ai9, Ai6, Ai3, etc.).

Each of these tools, however, come with their own set of caveats. *Post-hoc* immunohistochemistry will reliably label TH^+ cells however will result in false-negatives in neurons which have undergone extensive whole-cell recording times (Margolis et al., 2006). RetroBeads allows the user to surgically inject a

fluorescently labeled microsphere within a region of interest. These beads will then be transported in a retrograde fashion, which allows the user to select cell bodies of interest in the appropriate projection neurons. This trafficking takes time, however, and the user must wait weeks for the RetroBeads to travel to the cell bodies of interest. Fluorescently-labeled cholera toxin is another form of retrograde labeling that requires surgical intervention. Viral expression, however, is quick (on the order of days) but is toxic to cells over a long period of time. The advent of mouse reporter lines have allowed for the engineering of promoters of interest (e.g. TH and DAT) to be fused with fluorescent reporters which are long lasting within the mouse *in vivo*. Transgenic reporters, along with other reporter lines that are CRE dependent such as the Ai9 reporter (STOP-floxed-tdTomato), allow the user to combine a CRE line of interest to fluorescently label those cells upon recombination. There are a few considerations when selecting a CRE line for experimental use, once being that once the CRE has performed the recombination event, those cells will express the fluorophore for the lifetime of the animal and thus the expression of the reporter may not be representative of protein expression at the time the animal is sacrificed. In addition, the TH^{CRE} lines have come under much scrutiny as of late and it has been shown that TH^{CRE} lines exhibit low dopamine specificity whereas the DAT^{CRE} lines exhibit high dopamine specificity within the ventral midbrain (Lammel et al., 2015). Using a combinatorial approach of cell-type specific selection along with anatomical boundaries provides the best current approach for selecting DA neurons for electrophysiological characterizations.

1.2.3 Dopaminergic activity during reward and aversion

A topic of increasing interest is how DA efferents originating in the VTA encode two distinct behaviors: motivational salience/value and avoidance. Dopaminergic neurons have been classically defined to have a role in "reward-prediction error" that aids in positive-reinforcement learning (Schultz, 2007). Wolfram Schultz found that if a reward is larger than predicted, then DAergic neurons are strongly excited, but, if a reward is smaller than predicted then DAergic neurons are inhibited. In addition, if a reward is just as predicted, then this has no consequence on DA release. Moreover, DA neurons encode for "temporal difference error" (TDE) that is essential for positive-reinforcement learning and takes external sensory cues into account (Bromberg-Martin et al., 2010). In the case of TDE, DA neurons are excited when an external cue designates an increase in the value of a future reward; neurons are inhibited when an external cue designates a decrease in value of a future reward; and have little to no response when an external cue does not convey any new information for a future reward (Bromberg-Martin et al., 2010; Montague et al., 1996). In regards to motivational value and salience, reward and avoidance are often coupled together. For instance, if an animal is reward-seeking it has assigned a positive value to that reward but, if a reinforcing cue is aversive, it has assigned negative value to that cue. This has been defined as motivational *value* whereas, motivational *salience* refers to the attending of

particular cues that triggers the cognitive process for reward-seeking or avoidance (Bromberg-Martin et al., 2010).

But how are these behaviors encoded on a neuronal level? With the advent of optogenetics, and the use of *in vivo* single unit recordings, circuit-level processing for these two behaviors is becoming elucidated. *In vivo* electrophysiological recordings have shown that DA neurons change their firing frequency from a low, tonic frequency pattern to a high, phasic firing pattern to encode reward-prediction and motivational salience (Tsai et al., 2009). In contrast, these neurons are inhibited upon the presence of an aversive stimulus. While the correlation between DAergic activity and reward valence is tantalizing, these studies did not provide a causative link between the two. Causal links were first established using optogenetic approaches. For example, Tsai and colleagues performed experiments in which they injected a CRE dependent channel rhodopsin-2 (DIO-ChR2-EYFP) within the VTA of TH^{CRE} positive animals and tested them in a conditioned place preference paradigm (CPP). ChR2 allows for the precise control of the neurons of interest (on the order of ms) and in this case, provides the additional precision of manipulating a selected cell-type of interest (e.g. TH^+). This provided the first evidence that the activation of dopaminergic cell bodies alone results in behavioral conditioning by firing TH^+ neurons at a phasic firing frequency (50 Hz). In addition, this seminal paper illustrated that only phasic activation of TH^+ neurons results in robust DA release (~76 nM) within the NAc whereas tonic stimulation (1 Hz) results in incredibly low amounts of DA release (~1.5 nM) that correlate with the optically-evoked conditional place preference.

1.2.4 Targets of the VTA that promote reward-seeking: NAc, mPFC, and dorsal striatum

The mesolimbic pathway has long been associated with reward-seeking behavior. As mentioned in section **1.2.2**, phasic DA bursts from the VTA in several regions of the ventral and dorsal striatum encode reward-seeking behavior. However, the VTA has also been implicated in encoding avoidance therefore, DAergic phasic bursts to particular targets play an important role in encoding behavioral output. What are the differences within VTA target structures that encode these opposing behaviors? The striatum is a heterogeneous structure that is composed of three major cell types: medium spiny neurons (MSN), cholinergic interneurons, and GABAergic interneurons. Notably, the NAc is composed of approximately 95% MSNs that are further categorized by being either D1 or D2 containing (Robison and Nestler, 2011). D1 and D2 receptors have been shown to activate two different striatal circuits: the direct and indirect pathway, respectively. The direct pathway is known to play a key role in movement initiation, whereas the indirect pathway plays a role in inhibiting unwanted voluntary movements (Frank, 2005). The increase in DA concentration that results from phasic firing has been hypothesized to produce conditions of high available DA which preferentially activates D1 receptors and therefore causes activation of the direct pathway which facilitates movements towards a highly-valued reward (Bromberg-Martin et al., 2010; Frank, 2005). In conditions where DAergic neurons are inhibited (e.g. low-valued rewards), available DA will be low, inhibiting D2-containing neurons and initiating

suppression of movement via the indirect pathway (Bromberg-Martin et al., 2010; Frank, 2005). Further evidence for this is seen in optogenetic mediated CPP that is enhanced by cocaine. Optogenetic stimulation of D1 containing MSNs has shown to result in enhanced CPP when cocaine is on board whereas, stimulation of D2 containing MSNs has the opposite effect (Russo and Nestler, 2013). In addition, chronic administration of cocaine has been well described to have a role in structural and functional plasticity within MSNs, an effect that is illustrated by the increase in dendritic spine number and change in morphology (Russo and Nestler, 2013). There is a vast literature present on DAergic responses to reward from the VTA, however, there is still little evidence on how reward-seeking behavior is encoded to VTA accumbal targets. What has come to light is that DA is most important when target neurons are most excitable but, has little consequence otherwise (Floresco, 2015). Therefore, instead of directly promoting reward-seeking, DA may potentially be responsible for augmenting responses from the VTA that are being driven additionally by upstream glutamatergic inputs such as the PFC, glutamatergic projections from the VTA, hippocampus, and BLA.

The dorsal striatum, like the ventral striatum, is composed of MSNs that are mostly D1 and D2 containing. Characteristically, this subdivision of the striatum is classified within the basal ganglia and has been extensively studied for its role in motor execution and planning. As briefly mentioned, these D1- and D2-containing MSNs compose the direct (“go”) and indirect (“no-go”) pathway, respectively. However, Keeler, Pretsell, and Robinson (2014) proposed a new, more specific role for these two pathways and defined it as the Prepare and Select (PAS) circuit

(Keeler et al., 2014). This PAS circuit suggests that D1-expressing MSNs prepare the circuit for the possible motor actions that can be taken while the D2-expressing MSNs further refine this to achieve a respective goal. D1 and D2 receptors have different binding affinities for DA. D1 receptors have low binding affinity for DA and are therefore more sensitive to phasic dopamine release whereas, D2 receptors have high binding affinity for DA and are sensitive to tonic dopamine release (Dreyer et al., 2010; Keeler et al., 2014; Surmeier et al., 2007). These MSNs accumulate inputs from multiple regions (excitatory and dopaminergic) to then dictate a behavioral consequence. Each are responsive to DA, so how are these two distinct neuron types that respond to the same neuromodulator promote separate behavioral outcomes? The “race” hypothesis takes these binding affinities into account and proposes that D1 activation reduces the firing threshold which activates the “go” pathway preferentially; D2Rs are inhibitory and will therefore increase the input strength needed to activate the “no-go” pathway (Keeler et al., 2014). Because D1Rs are preferentially activated, they will encode more salient information and promote faster reaction times (Keeler et al., 2014). As an example, once an animal under goes training in an operant conditioning paradigm, the longer the animal has been undergoing training the faster reaction times will be even though the incoming sensory information is identical to previously experienced sessions. Therefore, D1Rs are thought to be preferentially activated in the presence of a highly-valued reward which is correlated with high striatal activity mediated by stimulatory g-coupled proteins. Repeated phasic dopamine release causes D1 and D2 receptor internalization (Ostlund et al., 2011). High reward-value is also encoded by D2Rs (in

addition to D1Rs) via internalization mechanisms and is correlated by the presence of low D2R expression. In the presence of a motivating stimulus (e.g. hunger or sex) tonic DA concentration is increased and will therefore, activate more D2Rs and in turn cause their internalization, biasing reward-seeking via D1R activation upon the presentation of a reward (Dreyer et al., 2010; Rice and Cragg, 2008).

The mesocortical pathway is composed of projections from the VTA to the PFC. These dopaminergic projections also have a long standing association with the reward-seeking pathway. However, these DA projections are not intrinsically rewarding *per se* but rather regulate essential circuits that are imperative for motivation such as higher-order motor control, motivation, and cognition (Seamans and Yang, 2004). DA release within the PFC is not related to reward-prediction error as in the NAc but rather plays an important role when the animal is performing the task. For instance, in a delayed response task, DA is released at the beginning of the task and is maintained during the performance of the task, suggesting that DA is required for the encoding and the use of working memory but is not necessary for retention of the task or to encode reward-value (Seamans and Yang, 2004). In primates, *in vivo* single-unit recordings in conjunction with microinontophoresis have provided empirical evidence that DA levels are the highest within the PFC during the delayed-period and that this effect of DA was mediated by D1 receptors specifically (Sawaguchi and Goldman-Rakic, 1994; Seamans and Yang, 2004). Lammel et. al. (2008) suggested that the VTA neurons which project to the PFC arise from a unique population within the medial posterior PFC and exhibit different electrophysiological properties as described in section **1.2.2**. In addition to the PFC

participating in reward-seeking by modulating working-memory, the PFC also plays an integral part in the extinction of a learned behavior associated with a reward (Sparta et al., 2014) that also consists of an active learning process. The mPFC is known to play a role in both appetitive and aversive conditioning and is the crucial circuit node for the expression and extinction of cue-mediated behaviors. Sparta and colleagues showed that this is a phenomenon that is likely mediated by parvalbumin positive fast-spiking interneurons (Sparta et al., 2014). The mesolimbic, mesocortical, and striatal circuits are therefore integral nodes for the expression, execution, acquisition, and extinction for motivation and reward-seeking.

1.2.5 Newly appreciated roles of dopamine and basal ganglia circuitry

Dopamine is the neuromodulator most strongly linked to reward prediction error (Schultz, 1998). However, basal ganglia / dopaminergic circuitry have also been strongly linked to reinforcement learning. Reinforcement learning, in the greater context of basal ganglia circuitry, is based on two different models of evaluation: model-based and model-free (Huys et al., 2015). Model-based evaluation is built on an animal's ability to create a probabilistic model of the world, which takes into account how predictive outcomes vary with the particular course of actions (Huys et al., 2015; Laurent and Balleine, 2015). On the other hand, model-free evaluation factors in how motivational states can introduce prediction errors that influence the ability to assess the long-range outcomes; chanegs in phasic dopamine release can alter these prediction errors (Huys et al., 2015). Taking these two models into account, goal-directed behavior has four separate elements:

(1) evaluation (e.g. value of an action), (2) execution (e.g. choosing an action), (3) acquisition (e.g. learning to perform so an action can be taken), and (4) interruption (e.g. interrupting a previously acquired behavior when a better alternative is available) (Laurent and Balleine, 2015). Three distinct basal ganglionic loops execute the four elements of goal directed behaviors. These loops are (i) motor loops, which initiates motor commands and occurs in both model-free and model-based evaluation. The (ii) cognitive loop, which plans actions and also occurs in both model-free and model-based evaluation. Lastly, the (iii) limbic loop which permits an action to be implemented given the motivational state of the animal. The pattern and amount of dopamine release influence the outcomes of these basal ganglionic loops, such that tonic dopamine release is thought to influence the utility of an action within these cases whereas, phasic dopamine release is thought to modulate reinforcement learning on a model-free basis (Huys et al., 2015; Laurent and Balleine, 2015).

In addition to the role of dopaminergic basal ganglia circuitry in goal directed behaviors, dopamine also has been shown to affect depressive mediated behaviors. Because DA has a long known role in reward-related motivational behaviors, Tye and colleagues used a cell type-specific excitation and inhibition of dopaminergic neurons to elucidate a mechanisms for bidirectionally modulating depressive symptoms (e.g. a decrease in escape behavior and sucrose consumption) (Tye et al., 2013). Conversely, channelrhodopsin-mediated excitation of VTA DA neurons increased escape attempts and sucrose consumption, suggesting that phasic dopamine bursts in the NAc are needed for escape-related behaviors. These

findings were the first to suggest an immediate role for phasic dopamine release in the bidirectional modulation of depressive symptoms caused by stressors, such as in a tail-suspension assay (Tye et al., 2013).

1.3 Dopaminergic phenotypes characterized neurodevelopmental models

Impaired social interactions, language deficits, and repetitive stereotyped behaviors are core phenotypes associated with autism (Geschwind and Levitt, 2007). Within these ascribed phenotypes, the hormone oxytocin has been elucidated to be an important social reinforcement signal within the NAc core (Dolen et al., 2013) and that polymorphisms of oxytocin receptors are associated with autism. While these findings do not directly implicate dopamine within autism spectrum disorders, they do provide novel contextual evidence for a decrease in appetitive (social) behavior within autism models that are mediated by D1/D2 receptor containing MSNs. However, many of the dopaminergic pathway dysfunctions characterized have centered on those phenotypes that are related to repetitive stereotyped behaviors and motor impairments. One intriguing finding was presented by the modeling of a single point mutation found within the human DAT (dopamine transporter) protein that is associated with ASD (Hamilton et al., 2013). The *de novo* missense mutation within hDAT (T356M) causes reverse transport of DA which results in an efflux and correlates with a potential increase in available extracellular DA which could account for some of the psychiatric symptoms seen in patients with ASDs (Hamilton et al., 2013).

1.3.1 Mouse models of 16p11.2 loss

16p11.2 is a common chromosomal mutation that has been associated with autism spectrum disorders (Portmann et al., 2014). Patients presenting with this chromosomal mutation have phenotypes much like those described within AS such as: motor deficits, speech/language delay, and severe cognitive impairments. Interestingly a duplication in 16p11.2 has been associated with schizophrenia (McCarthy et al., 2009; Portmann et al., 2014). The Dolmetsch group engineered a novel mouse line exhibiting a mutation within the syntenic region to the human homolog (Portmann et al., 2014). Using this neurodevelopmental mouse model, the deletion in 16p11.2 caused anatomical (within striatum and cortex) and neurophysiological abnormalities that could be correlated to motor dysfunction. These anatomical abnormalities included an increase in the number of D2 containing MSNs while exhibiting a decrease in D1-containing MSNs with no change in dendritic spine number. These 16p11.2 deletion mice exhibited a number of physiological changes specific to D2 containing MSNs including: increase sEPSC frequency, decrease paired pulse ratio (PPR), increase AMPA/NMDA ratio, and an increase in mEPSC frequency. Behavioral phenotypes that correlate with striatal dysfunction include decreased startle response, lack of movement fluidity, frequent tremor, frequent circling, and a decrease in exploration in an open-field context. Further validation of the D2R mediated effect was shown by the lack of an effect these mutant mice exhibited to pharmacological D2 antagonism. Overall, these results indicate that the loss of 16p11.2 results in anatomical changes that directly

affects motor dysfunction and is mediated by the loss of D1R containing MSNs and loss of Darpp-32, an integral DA signaling component.

1.3.2 Neuroligin-3 mutations associated with striatal dysfunction

Neuroligin is a post-synaptic cell-adhesion protein that modulates the formation of synapses. Mutations in neuroligin-3 (NL3) are associated with autism in humans and synaptic deficits in mice (Rothwell et al., 2014). There are several mouse models with various NL3 mutations that have no overlap in synaptic phenotypes but exhibit the same enhanced repetitive motor routines that are due to cerebellar or striatal deficits but not due to synaptic impairment within the NAc (Rothwell et al., 2014). Conditional deletion of NL3 in D1- and D2-containing MSNs increased rotorod learning by specifically impeding synaptic inhibition onto accumbal D1-containing MSNs but not D2-containing neurons. NL3 mutant mice had a decrease in intrinsic excitability, and increase in rheobase, and a decrease in AMPA/NMDA ratio in D1-containing MSNs (Rothwell et al., 2014). While these phenotypes were characterized within basal ganglia circuitry that receive robust dopaminergic inputs, they are not indicative of a direct dopamine deficiency.

1.3.3 Dopaminergic associated phenotypes in Rett syndrome

Mutations in MeCP2 (methyl CpG binding protein-2) causes Rett syndrome, an x-linked disorder that exhibits Parkinsonian-like tremors which is suggestive of nigrostriatal dysregulation (Gantz et al., 2011). This is evidenced by observing

conditional loss of MeCP2 within TH^+ neurons that is known to reduce locomotion (Samaco et al., 2009). Early in development (postnatal day 30), MeCP2 negative neurons exhibited decreases in dendritic length, resting membrane potential, and capacitance that was maintained in mature adults (> postnatal day 60) within the dorsal striatum. In addition, these neurons exhibited neurotypical D2R expression but altered D2R activation and a loss of DA release as measured by fast-scan cyclic voltammetry (Gantz et al., 2011).

CHAPTER 2

LOSS OF UBE3A FROM TH-EXPRESSING NEURONS SUPPRESSES GABA CO-RELEASE AND ENHANCES REWARD-SEEKING BEHAVIOR[1]

2.1 Overview

Motivated reward-seeking behaviors are governed by dopaminergic ventral tegmental area projections to the nucleus accumbens. In addition to dopamine, these mesoaccumbal terminals co-release other neurotransmitters including GABA, whose roles in regulating motivated behaviors are unknown. Here we demonstrate that specific loss of the Angelman syndrome-associated UBE3A protein in tyrosine hydroxylase-expressing neurons does not affect dopamine release, but impairs mesoaccumbal GABA co-release and enhances reward-seeking behavior.

2.2 Introduction

Loss-of-function of the maternal *UBE3A* allele causes Angelman syndrome (AS), a severe neurodevelopmental disorder characterized by cognitive impairments,

[1] This chapter was submitted to *Nature Neuroscience* on April 20, 2015 with Alice M. Stamatakis, Pranish A. Kantak, Zoe A. McElligott, Matthew C. Judson, Garret D. Stuber, and Benjamin D. Philpot.

epilepsy, lack of speech, and motor deficits (Williams et al., 2006). Some AS patients exhibit symptoms consistent with dopaminergic dysfunction (Dichter et al., 2012; Harbord, 2001), of which there is evidence in the mesoaccumbal pathway of AS model mice (*Ube3a*$^{m-/p+}$) (Riday et al., 2012). Notably, *Ube3a*$^{m-/p+}$ mice exhibit increased electrically-evoked dopamine release within the nucleus accumbens (NAc) and correlated enhancements in reward-seeking behavior in response to electrical stimulation of the medial forebrain bundle (Riday et al., 2012), suggesting that UBE3A may directly regulate dopamine release from mesoaccumbal terminals. Alternatively, extracellular activation of heterogeneous, non-dopaminergic projections within the medial forebrain bundle might lead to differential dopamine release through complex circuit-level mechanisms (Robinson et al., 2003). Here, we optogenetically interrogated putative roles for UBE3A in regulating neurotransmitter release from tyrosine hydroxylase-positive (TH^+) mesoaccumbal terminals and, in turn, motivational drive.

2.3 Results

To target catecholaminergic neurons and the mesoaccumbal pathway, mice expressing CRE recombinase within TH^+ neurons (*TH*^{CRE}) were crossed with *Ube3a*$^{m-/p+}$ mice or their wildtype littermates (*Ube3a*$^{m+/p+}$). To specifically manipulate the axon terminals of NAc-projecting TH^+ neurons, we transduced CRE-dependent AAV5-channelrhodopsin-2 fused to enhanced yellow fluorescent protein (ChR2-eYFP) into the VTA and implanted an optical fiber in the NAc (**Fig. 2.1a$_1$**). We observed qualitatively similar viral expression within the CRE-expressing lines (**Figs.**

2.1a$_2$, 2.2), but no expression following viral treatment in wildtype control mice. To determine how the loss of UBE3A affects reward-related phenotypes through TH$^+$ neurons projecting to the NAc, we tested mice in a real-time place preference task across a range of optical stimulation frequencies (20, 30, and 40 Hz) (**Fig. 2.3a**). When mice crossed into the designated stimulation side, light was constantly pulsed until they crossed back into the other side (Stamatakis and Stuber, 2012). *TH^{CRE}::Ube3a$^{m-/p+}$* mice showed a preference for receiving optical stimulation, regardless of stimulation frequency (**Fig. 2.3a$_{2-4}$**). This preference was statistically greater than that of both *TH^{CRE}::Ube3a$^{m+/p+}$* and wildtype mice at 30 Hz stimulation (**Fig. 2.3a$_3$**), and furthermore, did not coincide with a change in movement velocity (**Fig. 2.3b**). These data indicate that maternal *Ube3a* loss enhances reward-seeking behavior that is elicited by the selective optogenetic activation of TH$^+$ VTA-to-NAc terminals.

To determine if there are differences in positive-reinforcement behavior, we trained *TH^{CRE}::Ube3a$^{m-/p+}$* and *TH^{CRE}::Ube3a$^{m+/p+}$* mice to nose-poke for 30 Hz stimulation at a 1:1 fixed-ratio schedule. These mice similarly learned an appetitive nose-poke operant task (**Fig. 2.3c**). However, *TH^{CRE}::Ube3a$^{m-/p+}$* mice nose-poked to receive optical stimulation significantly more than *TH^{CRE}::Ube3a$^{m+/p+}$* mice (**Fig. 2.1b**). These data suggest that the loss of UBE3A enhances motivation driven through TH$^+$ terminals within the NAc, thus increasing reward-seeking.

Based on previous findings (Riday et al., 2012), we hypothesized that UBE3A loss might enhance optically-evoked reward-seeking by increasing VTA-to-NAc dopamine release. To examine this possibility, we performed *in vitro* fast-scan cyclic

voltammetry in brain slices from *TH^{CRE}::Ube3a$^{m-/p+}$* and *TH^{CRE}::Ube3a$^{m+/p+}$* mice expressing ChR2-eYFP within VTA-to-NAc terminals. To probe for possible changes in dopamine release and quantal content, we optically stimulated either with a single pulse (**Fig. 2.4a$_2$**) or with stimulation trains across a range of frequencies (**Fig. 2.4a$_3$**). Contrary to our initial hypothesis, the loss of UBE3A had no apparent effect on dopamine availability or release. Moreover, using *in vitro* whole-cell electrophysiology, we found that intrinsic excitability and inhibition onto VTA neurons were unchanged in *TH^{CRE}::Ube3a$^{m-/p+}$* mice compared to controls (**Fig. 2.5**). Collectively, these findings suggest that enhanced reward seeking in *Ube3a$^{m-/p+}$* mice is not due to changes in dopamine release from VTA-to-NAc dopaminergic terminals or due to altered excitability of dopaminergic VTA neurons in *Ube3a$^{m-/p+}$* mice.

Because VTA neurons exhibited typical excitability and retain a normal capacity to release dopamine in *Ube3a$^{m-/p+}$* mice (**Figs. 2.4-2.5**), we questioned if maternal *Ube3a* deletion selectively in catecholaminergic neurons would be sufficient to alter motivational drive. To test this, we used a novel conditional *Ube3a* knockout mouse (*Ube3a^{FLOX}*) to selectively delete maternal *Ube3a* in a *TH^{CRE}*-dependent manner (**Fig. 2.2**). We injected *TH^{CRE}::Ube3a$^{FLOX/p+}$* and *TH^{CRE}::Ube3a$^{m+/p+}$* mice with CRE-dependent ChR2-eYFP into the VTA to determine if deletion of *Ube3a* within TH$^+$ neurons would be sufficient to phenocopy reward-seeking phenotypes observed in AS model mice. Mice were trained to nose-poke (as described above) for optical stimulation of CRE$^+$ terminals within the NAc. *TH^{CRE}::Ube3a$^{FLOX/p+}$* mice poked significantly more for 30 Hz stimulation than

TH^{CRE}*::Ube3a*$^{m+/p+}$ mice (**Fig. 2.6a**). This difference occurred in the absence of observable changes in optically-evoked dopamine release (**Fig. 2.6b$_{1\text{-}2}$**). These data demonstrate that the selective loss of UBE3A in TH^{+} neurons is sufficient to enhance motivational drive despite the lack of a detectable deficit in NAc dopamine release.

In the NAc, dopaminergic terminals are capable of also releasing glutamate and GABA (Stuber et al., 2010; Tritsch et al., 2012; Tritsch et al., 2014; Zhang et al., 2015). Thus, we tested whether *Ube3a* loss in TH^{+} neurons could alter transmitter co-release. To assess this, we optogenetically activated VTA-to-NAc terminals and measured GABAergic currents in ventral striatal medium spiny neurons while blocking glutamatergic responses with AMPA and NMDA receptor antagonists (**Fig. 2.6c**). We applied a single light-pulse (20 ms) to measure peak amplitude and kinetics of the resulting current by averaging ≥ 6 consecutive traces (**Fig. 2.6d$_{1}$**). We confirmed *post hoc* that these currents were GABAR-mediated by bath applying SR95531, a selective GABA receptor antagonist (**Fig. 2.6d$_{1}$**). We found that GABAR-mediated currents in *TH*^{CRE}*::Ube3a*$^{FLOX/p+}$ mice showed a >50% reduction in peak amplitude relative to controls but displayed normal decay kinetics (**Fig. 2.6d$_{2\text{-}3}$**). Using an optical stimulation paradigm similar to that used in the behavioral experiments, we also found that *TH*^{CRE}*::Ube3a*$^{FLOX/p+}$ mice exhibit diminished GABAergic currents at 30 Hz stimulation of VTA-to-NAc terminals compared to control mice (**Fig. 2.6d$_{4}$**).

Collectively, our data indicate that UBE3A regulates circuits involved in reward-seeking behavior and, in particular, GABA co-release from putative dopaminergic mesoaccumbal terminals. Following UBE3A loss, suppressed GABA

co-release and enhanced reward-seeking behavior occur in the absence of other measured cellular and synaptic deficits in the mesoaccumbal pathway. This suggests that GABA co-release from VTA-to-NAc terminals may be causally linked to motivational drive in *Ube3a*-deficient mice.

2.5 Materials and Methods

2.5.1 Experimental Subjects and Stereotaxic Surgeries

Cg-Tg-TH:Cre mice (JAX #: 008601), *Rosa26-stop-floxed-tdTomato* (Ai9, JAX #: 007909), and *Ube3a*-deficient (JAX #: 016590) mice were obtained through Jackson Laboratories. *Ube3a-floxed* mice were engineered in conjunction with the UNC Animal Models Core. These mice were on a C57BL/6 background except for the *Ube3a-floxed* mice which were mixed with a 129S6:C57BL/6 background but backcrossed eight generations before experimental use. Mice were housed on a 12:12 light-dark cycle. Mice for electrophysiological recordings were aged P60-P90 and were compared to wild-type age- and sex-matched controls. The experimenter was blind to genotype, and littermate controls were used when possible. Behavioral mice were group housed until surgery and were taken at 25-30g (approximately P60). Mice were anesthetized with ketamine (150mg/kg) and xylazine (50mg/kg), and then placed in a stereotaxic frame (Kopf Instruments) for bilateral injections (0.5µl) of purified adeno-associated virus (~10^{12} viral genomes/ ml, packaged and titered by the UNC Viral Vector Core Facility) into the VTA (coordinates from bregma: -3.15 anterior/posterior, ±0.75 medial/lateral, -4.75 dorsal/ventral). VTA

neurons in *TH*^{CRE} positive *Ube3a*$^{m-/p+}$, *Ube3a*$^{FLOX/p+}$, or *Ube3a*$^{+/+}$ mice were transduced with virus encoding ChR2-eYFP under the control of the *EF1α* promoter. Following surgery, mice were individually housed. For behavioral experiments, mice were implanted with bilateral chronic fibers directed above the NAc (coordinates from bregma: +1.2 A/P, ±1.6 M/L, -4.6 D/V at a 10°angle). We performed all experiments 5-8 weeks post-surgery. All procedures were conducted in accordance with the Guide for the Care and Use of Laboratory Animals as adopted by the National Institutes of Health, and with approval of the UNC Institutional Animal Care and Use committees.

2.5.2 Slice preparation for whole-cell electrophysiology and voltammetry

Mice were anesthetized with pentobarbital (40mg/kg) and intracardially perfused with ice-cold dissection buffer (in mM: 87 NaCl, 2.5 KCl, 1.25 NaH_2PO_4, 26 $NAHCO_3$, 75 sucrose, 10 dextrose, 1.3 ascorbic acid, 7 $MgCl_2$ and 0.5 $CaCl_2$) bubbled with 95% O_2-5% CO_2 after disappearance of corneal reflexes. Brains were then rapidly removed and immersed in ice-cold dissection buffer. VTA sections were dissected and 200μM horizontal slices were prepared using a vibrating microtome (Leica VT1200S). NAc sections were dissected and 250μM coronal slices were prepared as described within the VTA. Slices recovered for 20 min in a 35°C submersion chamber filled with oxygenated artificial cerebrospinal fluid (ACSF) (in mM: 124 NaCl, 3 KCl, 1.25 NaH_2PO_4, 26 $NAHCO_3$, 1 $MgCl_2$, 2 $CaCl_2$, and 20 glucose) and then kept at room temperature for >40 min until use (Philpot et al., 2003).

2.5.3 Voltage-clamp Recordings

Spontaneous Inhibitory Postsynaptic Currents: To isolate spontaneous inhibitory postsynaptic currents (sIPSCs), slices were placed in a submersion chamber, maintained at 27°C and perfused at 2 ml/min with oxygenated ACSF (as described above) and held at the AMPAR reversal potential (+10mV). AMPAR reversal potential was empirically determined by applying a series of 10 pA current injections (-70 to +60 mV) in the presence of picrotoxin and D,L-APV. sIPSCs were confirmed *post hoc* by the addition of 10μM SR95531. Cells were visualized using a Zeiss Examiner microscope equipped with infrared differential interference contrast (IR-DIC) optics. Putative VTA-to-NAc dopaminergic neurons were identified by *tdTomato* fluorescence medial to the medial terminal nucleus of the accessory optic tract in TH^{CRE}*::Ai9::Ube3a*$^{m-/p+}$ or wildtype mice. Patch pipettes were pulled from thick-walled borosilicate glass (P2000, Sutter Instruments Novato, CA). Open tip resistances were between 2.5-5 MΩ and were back-filled with an internal containing (in mM): 100 $CsCH_3SO_3$, 15 CsCl, 2.5 $MgCl_2$, 10 Hepes, 5 QX-314, 5 BAPTA, 4 Mg-ATP, 0.3 Mg-GTP, and 0.025 Alexa-488 with pH adjusted to 7.25 with 1M CsOH and osmolarity adjusted to ~295 mOsm by the addition of sucrose. Voltage-clamp recordings were performed in the whole-cell configuration using patch-clamp amplifier (Multiclamp 700B, Molecular Devices), and data were acquired and analyzed using pClamp 10 software (Molecular Devices). Pipette seal resistances were >1 GΩ, and pipette capacitive transients were minimized before breakthrough. Changes in series and input resistance were monitored throughout the experiment

by giving a test pulse every 30s and measuring the amplitude of the capacitive current. Cells were discarded if series resistance rose above 30 MΩ.

Optogenetic activation of TH^{CRE}::ChR2-eYFP fibers and measurement of GABA co-release: Widefield ChR2 mediated photostimulation was provided through a 20X/0.8 NA objective using single-photon excitation through a 470 nm λ filter. Light power was provided by a Lambda DG-4 300 W Xenon bulb (Sutter Instruments). This light was coupled to a Mosaic microelectro-mechanical-system digital micromirror device (Andor Technology) and was shuttered via pClamp mediated TTL pulse to the Lambda DG-4 as previously described (Larsen et al., 2014). GABA co-release from TH positive terminals originating in the VTA was measured in medium spiny neurons in response to a single 20 ms pulse as well as to a 1 s train of pulses at 30 Hz stimulation. Medium spiny neurons were identified by their shape and passive membrane properties (C_m, R_m, and decay constant) immediately after break-in in the voltage-clamp configuration holding at -70mV.

Activation of ChR2-expressing fibers was performed by using square illumination patterns (as described (Larsen et al., 2014)) in animals previously used in the optical ICSS paradigm. In response to these stimuli, mean IPSC amplitude, decay/rise tau, and total charge were measured by averaging ≥6 consecutive traces. Optical inhibitory postsynaptic currents (oIPSCs) were measured in ventral striatal MSNs which were selected by their membrane properties. oIPSCs were isolated by including DNQX (20 μM) and DL-APV (100 μM) in the external solution. Patch

pipette open-tip resistances were between 2.5-6 MΩ and were backfilled with (in mM): 125 CsCl, 10 TEA-Cl, 0.1 EGTA (Cs-OH), 10 Hepes, 3.3 QX314, 1.8 $MgCl_2$, 4 ATP, 0.3 GTP, 8 Na_2-Phosphocreatine with pH adjusted to 7.25 with 1M CsOH and osmolarity adjusted to ~295 by the addition of sucrose. The high internal chloride concentration increased the chloride driving force and allowed for oIPSCs to be more easily resolved at -70 mV. Changes in series and input resistance were monitored throughout the experiment and did not differ between genotypes ($p>0.05$). Recordings were discarded if series resistance rose above 30 MΩ.

2.5.4 Current-clamp Recordings

Intrinsic excitability experiments were performed at -50 to -60 mV in ACSF containing picrotoxin (50 μM), DNQX (20 μM), and DL-APV (100 μM) to block excitatory and inhibitory transmission. Putative VTA-to-NAc dopaminergic cells were selected as described above and pipettes were backfilled with (in mM): 100 K-gluconate, 20 KCl, 10 Hepes, 0.2 EGTA, 4 ATP, 0.3 GTP, 10 Na_2-Phosphocreatine, and 0.015 Alexa-488 with pH adjusted to 7.25 with 1M KOH and osmolarity adjusted to ~295 by the addition of sucrose. For frequency-current plots, current was injected at 40 pA steps and average AP frequency was calculated to the same current injection. Peak amplitude was calculated by averaging the max amplitude for all events across all collected traces. Max instantaneous frequency was calculated by taking the inverse of the shortest inter-event interval across all collected traces. Changes in series and input resistance were monitored throughout the experiment

by giving a test pulse every 30s and measuring the amplitude of the capacitive current. Cells were discarded if series resistance rose above 30 MΩ.

2.5.5 Fast-scan Cyclic Voltammetry

Ventral striatum sections were prepared as described above. Electrochemical data were acquired using a custom-written software in LabVIEW (Tar Heel CV) and filtered at 1 kHz offline. Briefly, carbon fiber microelectrodes (50 μM in length) were scanned from -0.4 V to 1.3 V at a rate of 400 V/s. Samples were acquired at a rate of 10 Hz. Light pulses (5 ms, 473 nm, 1 mW) were delivered through a 40X objective via a high-powered LED (Thorlabs) to evoke dopamine release. A single pulse or 5 light pulses were delivered at 1, 5, 10, 20, 30, and 40 Hz in a randomized order. Immediately after optical stimulation of the slice, background-subtracted cyclic voltammograms were generated, which were characteristic of dopamine (peak oxidation potential of 600-700 mV). For complete methods please see (Stamatakis et al., 2013).

2.5.6 Immunohistochemistry

Mice were anesthetized with pentobarbital and then perfused with 4% paraformaldehyde in PBS (pH ~7.3). Samples were placed in 10, 20, and then 30% sucrose in PBS before being cut at 40 μM using a cryostat (Leica). Sections were collected, rinsed (PBS), and blocked with 5% normal goat serum and 0.2% Triton X-100 in PBS. Sections were then tumbled in this blocking solution with primary antibody for 24 hours at 4°C. The primary antibodies used in this study were rabbit

anti-TH (1:650 Millipore, AB152), chicken anti-EGFP (1:1000 Aves), and mouse anti-UBE3A (1:750 Sigma clone 3E5, SAB1404508). Transgenic fluorescent proteins expressed via *CRE*-mediated recombination (Ai9 mice) were not further antibody enhanced. Secondary detection was performed with Alexa Fluor 488, 568, or 633 conjugated goat anti-rabbit, anti-chicken, or anti-mouse antibodies (Invitrogen). Mounted sections were imaged on a Zeiss LSM 710 Confocal Microscope using 20X/0.8, or 40X/1.3 NA objectives. Immunohistochemistry was used to validate viral injection, fiber placement, and recombination efficiency post-hoc in experimental animals.

2.5.7 *In vivo* optogenetic excitation

For all behavioral experiments, mice were injected with AAV5-EF1α-DIO-ChR2-eYFP virus and implanted with bilateral custom-made optical fiber targeted to the NAc core (Sparta et al., 2012). Mice were connected to a 'dummy' optical patch cable 5 days before the experiment each day for 60 min to habituate them to the tether procedure. Following the tethering procedure, we ran the mice in several behavioral procedures (detailed below). We used a 10 mW, 473 nm laser with a stimulation frequency of 30 Hz and a 5 ms pulse width duration for all behavioral assays unless otherwise noted.

2.5.8 Real-time Place Preference

Mice were placed in a behavioral arena (50 x 50 x 25 cm black) for 20 min. One side (counterbalanced) of the chamber was paired with optical stimulation.

Mice were initially placed in the nonstimulation side at the onset of the experiment and were delivered a 5, 10, 20, 30, 40, or 60 Hz (randomized) constant laser stimulation each time the mouse crossed to the stimulation side of the chamber until the mouse crossed back into the nonstimulation side. We recorded behavioral data via a CCD camera interfaced with Ethovision XT software (Noldus Information Technologies). Mice underwent one session per day during their respective dark cycle.

2.5.9 Positive reinforcement procedures and Optical Self-Stimulation

Behavioral training and testing occurred in mouse operant chambers (Med Associates) interfaced with optogenetic stimulation equipment. Behavioral paradigms were performed during their respective dark cycle. Food restricted male mice (90% of their free-feeding bodyweight) were trained on a fixed ratio (1:1) training schedule for one session per day for 60 min, in which each nose poke resulted in 20 µl of a 15% sucrose administration until the number of nose pokes did not vary >20% across three consecutive days. In addition, active nose poke ports were coupled with a cue light that remained on. With each successful nose poke, the cue light turned off and a tone would be presented for 3 s. Once the mice reached a stable number of nose pokes, they were habituated for 5 consecutive days to the patch cable with optical stimulation (3 s of 30 Hz) time-locked to the cue following each active nose poke. After the 5 day habituation phase, mice were then tested following a 2 day break. Active and inactive nose pokes were recorded in addition to time-stamps.

2.5.10 Statistics and Data Analysis

We plotted all data and performed all statistical analyses on GraphPad Prism software. All graphs are represented as the mean ± SEM. For statistical analyses, we used two-way ANOVA (**Figs. 2.1b$_2$, 2.6a-b$_2$, 2.4a$_3$**), one-way ANOVA (**Fig. 2.6a$_2$-b**), or two-tailed student's t-test (**Fig. 2.6d$_{2\text{-}4}$, 2.3c$_2$, 2.4a$_2$, and 2.5**). Statistical significance is represented as follows: *p<0.05, **p<0.02, and ***p<0.001. Minimum sample sizes were estimated from previously published data sets with similar experimental parameters. The only data points that were discarded were done so before unblinding and only because the data points did not meet *a priori* criteria for data inclusion (e.g. – series resistance in a whole-cell recording was above our established limit for inclusion). No outlier test was used to discount any data point, and all data points were included within the summarized graphs.

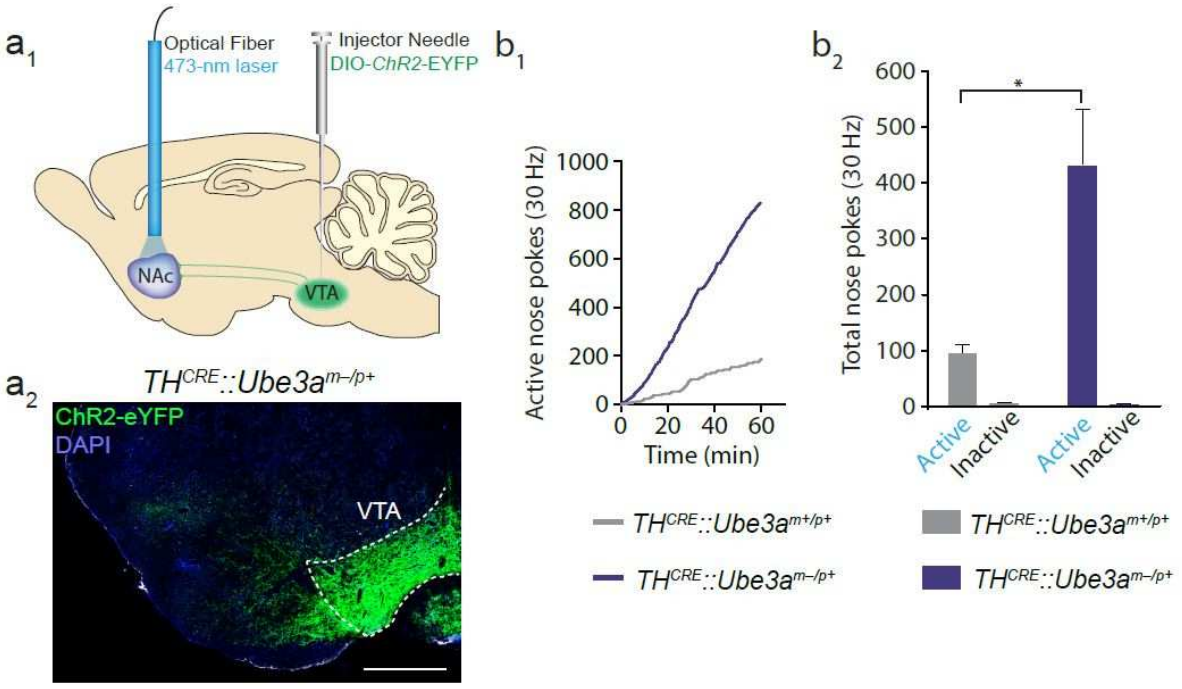
a1
Optical Fiber
473-nm laser
Injector Needle
DIO-ChR2-EYFP
NAc
VTA
a2
THCRE::Ube3am–/p+
ChR2-eYFP
DAPI
VTA
b1
Active nose pokes (30 Hz)
Time (min)
THCRE::Ube3am+/p+
THCRE::Ube3am–/p+
b2
Total nose pokes (30 Hz)
Active
Inactive
Active
Inactive
THCRE::Ube3am+/p+
THCRE::Ube3am–/p+

Figure 2.1: *Ube3a*$^{m-/p+}$ mice are hyper-motivated to self-stimulate TH-positive VTA-to-NAc terminals.

(**a**$_1$) Schematic representation of DIO-ChR2-eYFP viral transduction within the VTA along with NAc chronic fiber placements into *TH*^{CRE}-positive mice. (**a**$_2$) Immunohistochemistry of ChR2-eYFP (green), and DAPI (blue) in a *TH*^{CRE} *::Ube3a*$^{m-/p+}$ mouse. Scale bar = 500 µM. (**b**$_1$) Cumulative response plots showing cumulative nose pokes that trigger a 30 Hz, 473 nm stimulus (active nose pokes) in representative mice. (**b**$_2$) Average number of nose pokes for triggering (active nose pokes) or not triggering (inactive) 30 Hz optical stimulation across a 60 minute session. *TH*^{CRE}*::Ube3a*$^{m-/p+}$ mice were significantly more motivated to trigger optical stimulation than *TH*^{CRE}*::Ube3a*$^{m+/p+}$ mice (n=7 for each group,*p<0.05). All bars represent the mean ± SEM.

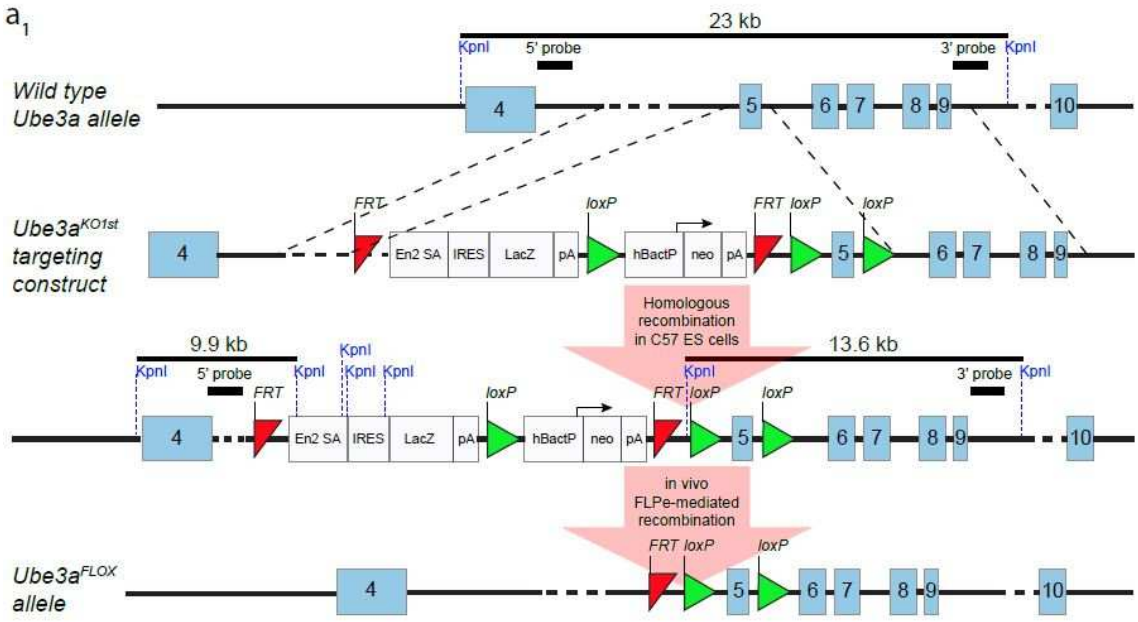
a1
23 kb
KpnI
5' probe
3' probe
KpnI
Wild type
Ube3a allele
4
5
6
7
8
9
10
FRT
loxP
FRT loxP
loxP
Ube3aKO1st
targeting
construct
En2 SA
IRES
LacZ
pA
hBactP
neo
pA
Homologous
recombination
in C57 ES cells
9.9 kb
13.6 kb
in vivo
FLPe-mediated
recombination
Ube3aFLOX
allele

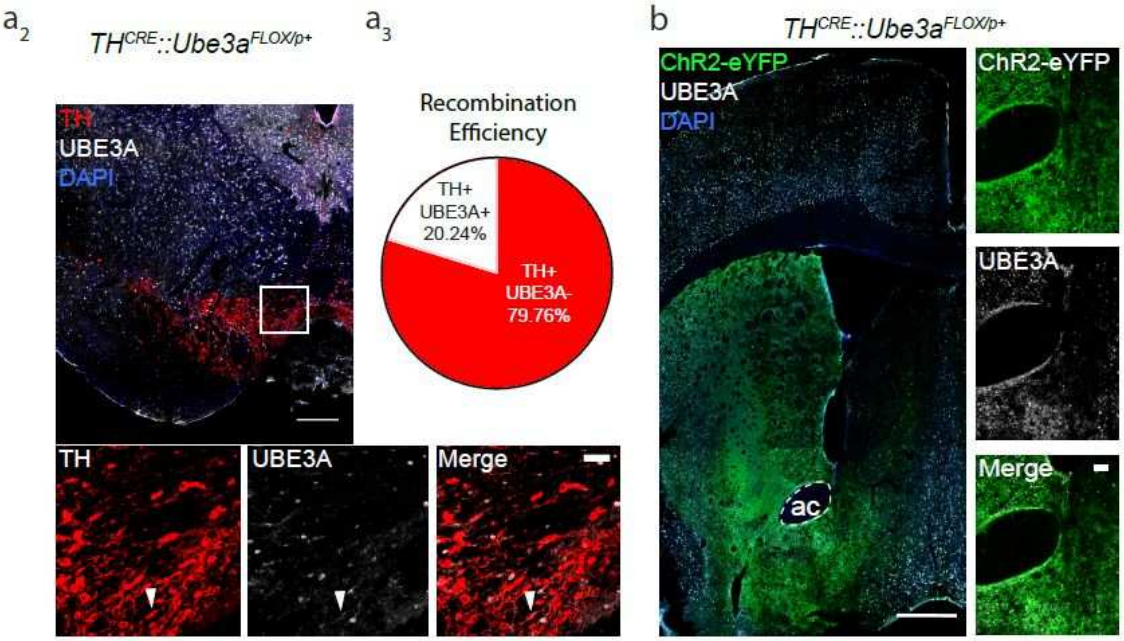
a2
THCRE::Ube3aFLOX/p+
TH
UBE3A
DAPI
a3
Recombination
Efficiency
TH+
UBE3A+
20.24%
TH+
UBE3A-
79.76%
TH
UBE3A
Merge
b
THCRE::Ube3aFLOX/p+
ChR2-eYFP
UBE3A
DAPI
ac

Figure 2.2: *TH^{CRE}*-mediated recombination of the maternally inherited *Ube3a^{FLOX}* allele abolishes UBE3A within VTA but not striatal neurons.

(**a$_1$**) Schematic of strategy used to generate C57BL/6 mice carrying the *Ube3a^{FLOX}* allele. Note that these mice have been fully anatomically and molecularly validated (Judson et al., in review). (**a$_2$**) Immunohistochemistry showing UBE3A-positive (white) and TH-positive (red) neurons in *TH^{CRE}::Ube3a$^{FLOX/p+}$* mice. Scale bar = 500μM (top) or 50μM (bottom). High magnification views are of area outlined by white box. Arrowhead represents residual UBE3A expression within a TH-positive neuron. (**a$_3$**) Quantification demonstrating a recombination efficiency of ~80% (n=2 mice). (**b**) Immunohistochemistry showing ChR2-eYFP (green), UBE3A (white), and DAPI (blue) in the striatum of *TH^{CRE}::Ube3a$^{FLOX/p+}$* mice following injection of DIO-ChR2-eYFP into the VTA. UBE3A expression is qualitatively similar to wild-type levels of UBE3A within the striatum. ac=anterior commissure.

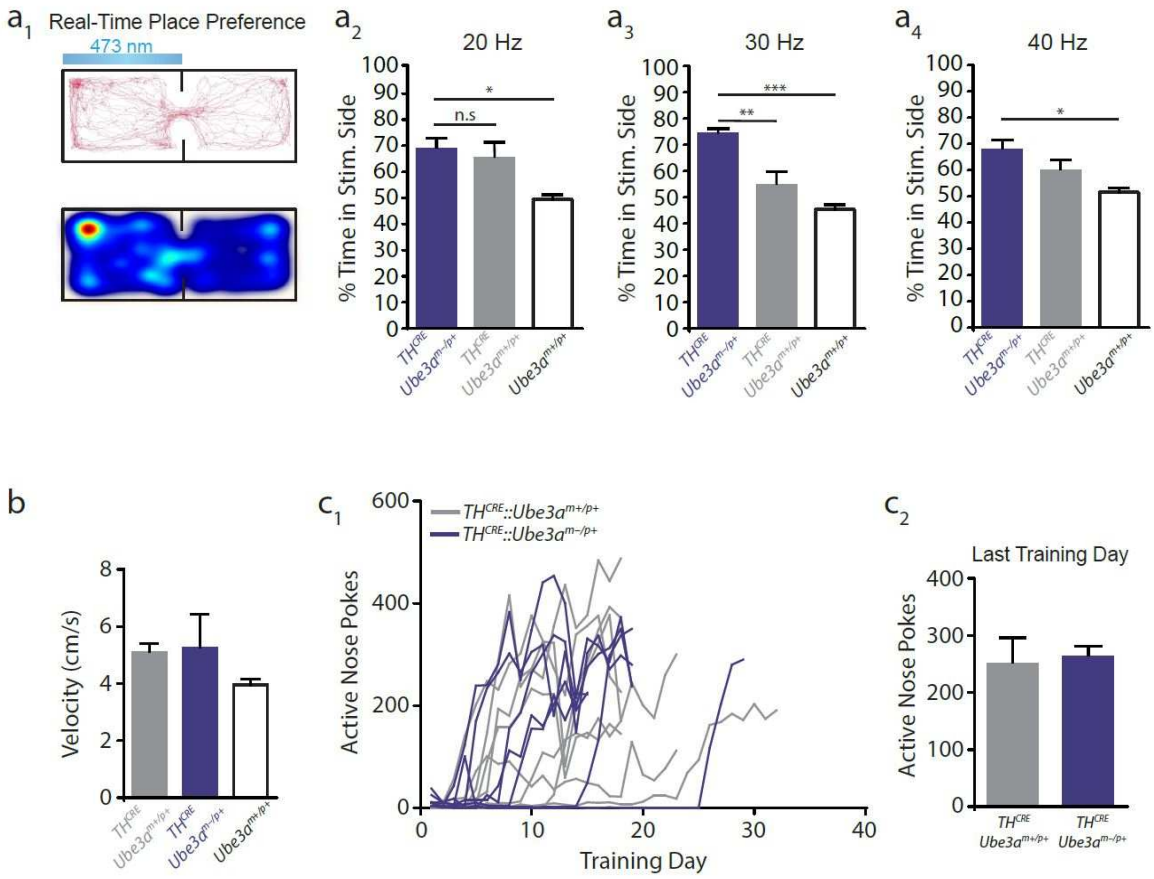
a1
Real-Time Place Preference
473 nm
a2
20 Hz
% Time in Stim. Side
n.s
*
a3
30 Hz
% Time in Stim. Side
**
***
a4
40 Hz
% Time in Stim. Side
*
THCRE Ube3am−/p+
THCRE Ube3am+/p+
Ube3am+/p+
b
Velocity (cm/s)
c1
THCRE::Ube3am+/p+
THCRE::Ube3am−/p+
Active Nose Pokes
Training Day
c2
Last Training Day
Active Nose Pokes

Figure 2.3: *TH^{CRE}::Ube3a$^{m-/p+}$* mice exhibit greater preference for stimulation of TH-positive VTA-to-NAc terminals than wild-type mice but learn on similar timescales.

(**a**) Wire frame and heat plots representing a single mouse's movements in real-time place preference arena during a 20 min session. (**a$_{2-4}$**) Average data showing % time *TH^{CRE}::Ube3a$^{m-/p+}$*, *TH^{CRE}::Ube3a$^{m+/p+}$,* and *TH^{CRE}* negative control mice spent in side triggering optical stimulation at 20, 30, or 40 Hz (p's<0.05). (**b**) Mean velocity in *TH^{CRE}::Ube3a$^{m-/p+}$*, *TH^{CRE}::Ube3a$^{m+/p+}$,* and *TH^{CRE}* negative controls (n=5/genotype). (**c$_1$**) Plot showing active nose pokes for each mouse across sucrose training days. (**c$_2$**) Average number of nose pokes performed on the last sucrose training day for *TH^{CRE}::Ai9::Ube3a$^{m-/p+}$* and *TH^{CRE}::Ai9::Ube3a$^{m+/p+}$* mice (p=0.84). Bars represent mean ± SEM.

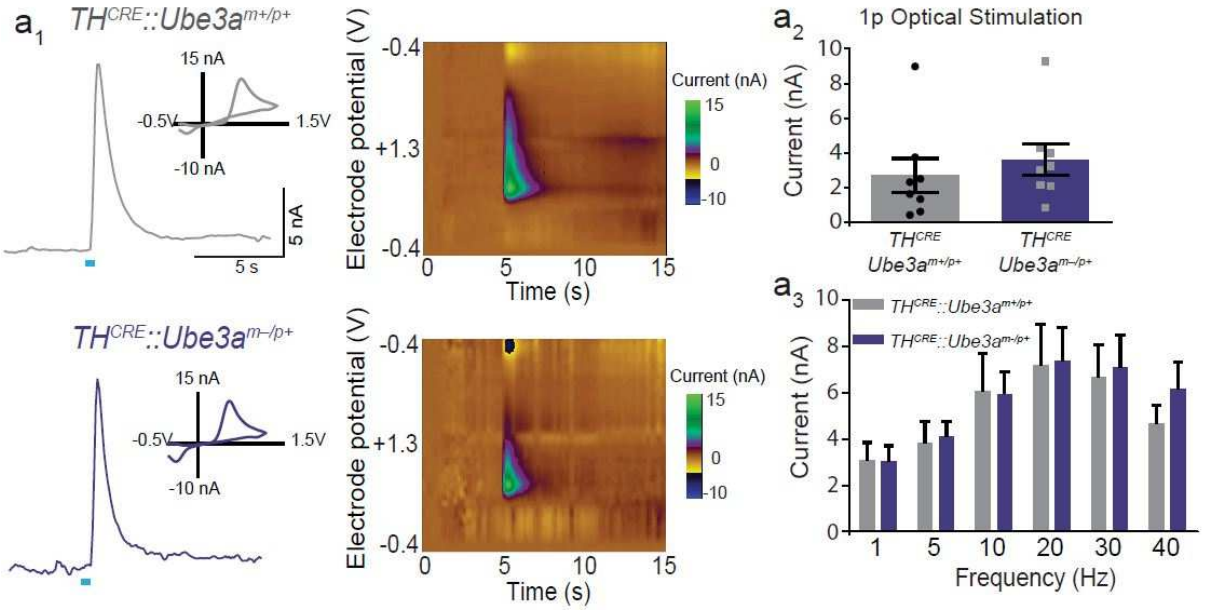

Figure 2.4: Optically evoked dopamine release is similar in TH-positive VTA-to-NAc terminals in *Ube3a*$^{m-/p+}$ and *Ube3a*$^{m+/p+}$ mice.

(**a$_1$**) Representative fast-scan voltammetric recordings from ventral striatal slices in both *TH*^{CRE}*::Ube3a*$^{m-/p+}$ and *TH*^{CRE}*::Ube3a*$^{m+/p+}$ mice. Insets represent background subtracted electrochemical signal characteristic of oxidized dopamine. Right: Consecutive background subtracted voltammogram recorded over an 8-s interval. Applied electrode potential (E_{apps} vs. Ag/AgCl reference electrode) is shown versus time. (**a$_2$**) Light-evoked current is similar in both genotypes at 1-pulse ($p=0.99$, $n=8, 9$) and (**a$_3$**) across a range of frequencies ($p= 0.83$, $n=11, 12$).

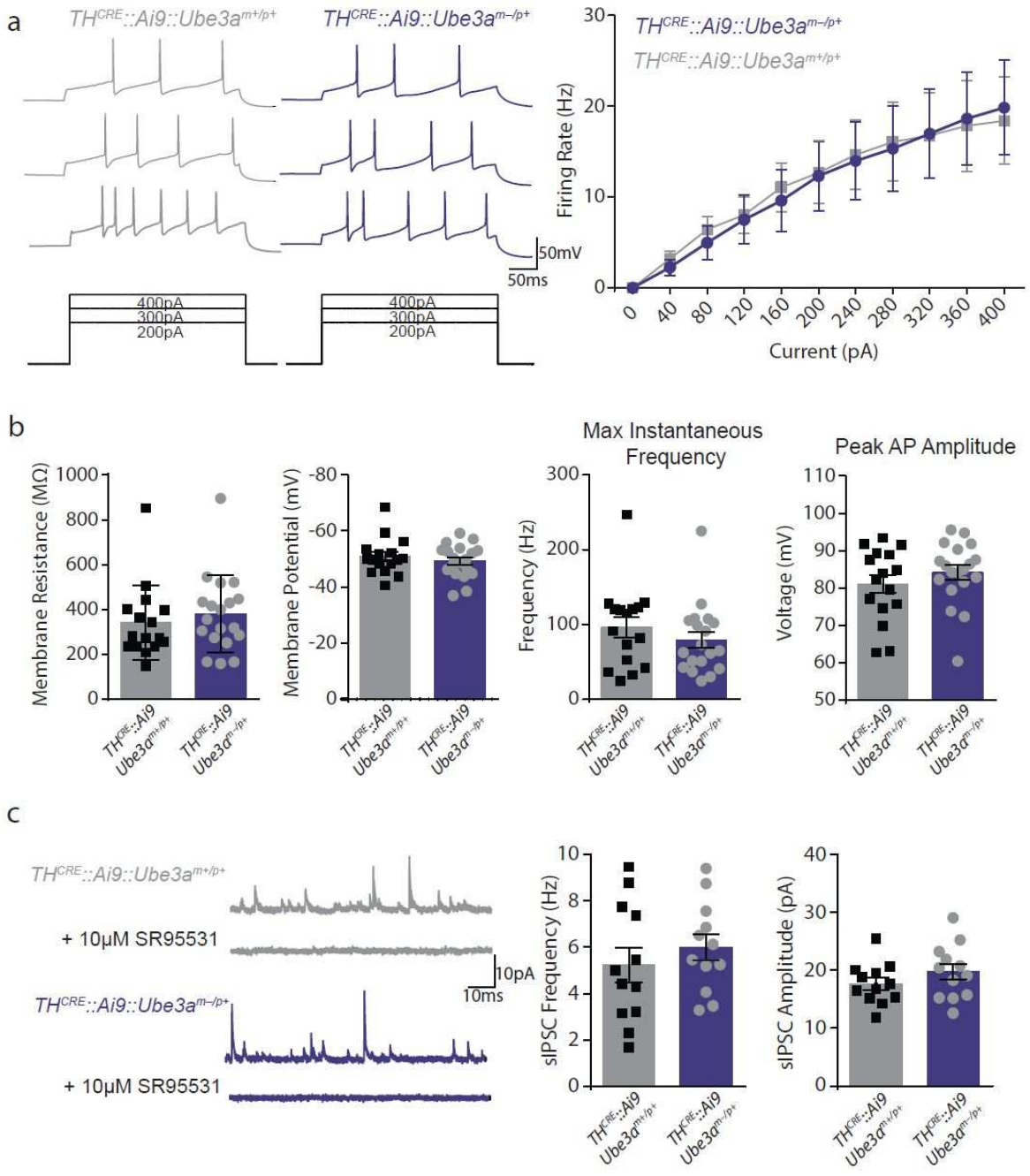
a
THCRE::Ai9::Ube3am+/p+
THCRE::Ai9::Ube3am−/p+
50mV
50ms
400pA
300pA
200pA
Firing Rate (Hz)
Current (pA)
b
Membrane Resistance (MΩ)
Membrane Potential (mV)
Max Instantaneous Frequency
Frequency (Hz)
Peak AP Amplitude
Voltage (mV)
c
+ 10μM SR95531
10pA
10ms
sIPSC Frequency (Hz)
sIPSC Amplitude (pA)

Figure 2.5: Maternal deletion of *Ube3a* in TH-positive neurons has no apparent effect on intrinsic excitability and inhibitory input onto VTA neurons.

(**a**) Representative traces and average data showing action potential firing rates to increasing current injections in Ai9-positive VTA neurons in *TH^{CRE}::Ai9::Ube3a$^{m-/p+}$* and *TH^{CRE}::Ai9::Ube3a$^{m+/p+}$* mice (n=18/ group, p=0.70). (**b**) Average values of resting membrane potential (p=0.46), membrane resistance (p=0.25), maximum instantaneous firing frequency (p=0.22), and average action potential (AP) peak amplitude (p=0.32) of Ai9-positive neurons. (c) Representative traces and average data showing spontaneous inhibitory postsynaptic currents (sIPSCs) in Ai9-positive neurons (n=12 for each genotype, p=0.42, p=0.24). GABAergic currents were validated by bath application of SR95531. All bars represent mean ± SEM.

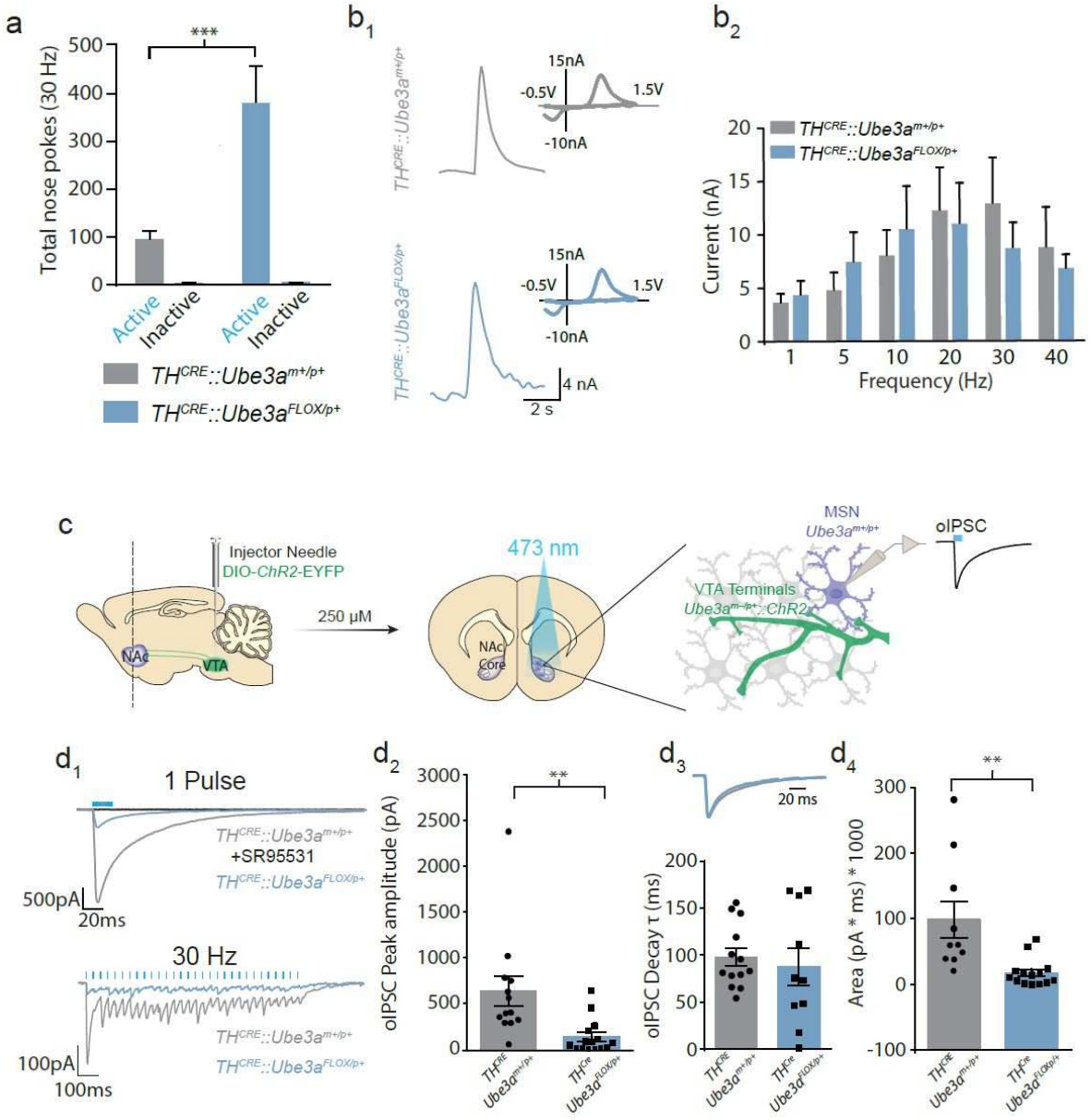
a
***
Total nose pokes (30 Hz)
500
400
300
200
100
0
Active
Inactive
Active
Inactive
THCRE::Ube3am+/p+
THCRE::Ube3aFLOX/p+
b1
THCRE::Ube3am+/p+
15nA
-0.5V
1.5V
-10nA
THCRE::Ube3aFLOX/p+
15nA
-0.5V
1.5V
-10nA
4 nA
2 s
b2
THCRE::Ube3am+/p+
THCRE::Ube3aFLOX/p+
Current (nA)
20
15
10
5
0
1
5
10
20
30
40
Frequency (Hz)
c
Injector Needle
DIO-ChR2-EYFP
250 µM
NAc
VTA
473 nm
NAc Core
MSN
Ube3am+/p+
VTA Terminals
Ube3am−/p+::ChR2
oIPSC
d1
1 Pulse
THCRE::Ube3am+/p+
+SR95531
THCRE::Ube3aFLOX/p+
500pA
20ms
30 Hz
THCRE::Ube3am+/p+
THCRE::Ube3aFLOX/p+
100pA
100ms
d2
**
oIPSC Peak amplitude (pA)
3000
2500
2000
1500
1000
500
0
THCre Ube3am+/p+
THCre Ube3aFLOX/p+
d3
20 ms
oIPSC Decay τ (ms)
200
150
100
50
0
THCre Ube3am+/p+
THCre Ube3aFLOX/p+
d4
**
Area (pA * ms) * 1000
300
200
100
0
-100
THCre Ube3am+/p+
THCre Ube3aFLOX/p+

Figure 2.6: Deleting *Ube3a* in TH-positive neurons decreases GABA co-release and is sufficient to enhance motivational behavior.

(**a**) Average nose pokes for inactive and active ports triggering 30 Hz optical intracranial self-stimulation in a 60 minute behavioral session (n=5 and 7, *p<0.02). Experimental design was similar to that schematized in Figure 1a$_1$, except that *TH^{CRE}::Ube3a$^{FLOX/p+}$* and *TH^{CRE}::Ube3a$^{m+/p+}$* mice were examined to selectively delete *Ube3a* and optically stimulate TH$^+$ VTA-to-NAc terminals. (**b$_1$**) Representative fast-scan cyclic voltammograms assessing dopamine release within the ventral striatum of *TH^{CRE}::Ube3a$^{FLOX/p+}$* and *TH^{CRE}::Ube3a$^{m+/p+}$* mice. Dopamine release was evoked by 30 Hz (5-pulses) optical stimulation. Insets represent background subtracted electrochemical signal characteristic of oxidized dopamine. (**b$_2$**) Averaged optically-evoked dopamine release at a range of frequencies demonstrates that there are no statistical differences between genotypes (n=6 and 7, p>0.05). (**c**) Schematic representing protocol for whole-cell optical IPSC (oIPSC) recordings within the NAc of *TH^{CRE}::Ube3a$^{FLOX/p+}$* mice. IPSCs were pharmacologically isolated (see Methods). (**d$_1$**) Representative oIPSC traces measured in *TH^{CRE}::Ube3a$^{FLOX/p+}$* and *TH^{CRE}::Ube3a$^{m+/p+}$* mice and evoked by single pulses (20ms) or 30 Hz trains of stimulation. The pharmacological isolation of GABAergic currents was validated by application of the antagonist SR95531. (**d$_2$**) Average peak amplitude of single oIPSCs demonstrate a significant reduction of GABAergic currents in *Ube3a$^{FLOX/p+}$* mice (n=13 and 15, **p<0.05). (**d$_3$**) Average decay kinetics of oIPSCs analyzed in panel d$_2$ (p=0.61). Representative traces are shown with normalized amplitude to demonstrate similar current decay kinetics. (**d$_4$**) Average oIPSC charge evoked

using a similar 30 Hz optical stimulation paradigm employed behaviorally (see panel "a") and tested *in vitro* (bottom traces of "d_1"). *TH^{CRE}::$Ube3a^{FLOX/p+}$* animals showed a significant decrease in GABA co-release (n=10 and 14,**p<0.05). All bars represent the mean ± SEM.

CHAPTER 3

POTENTIAL MECHANISMS UNDERLYING HYPERMOTIVATION IN CELL TYPE-SPECIFIC LOSS OF UBE3A

The following chapter is subdivided into three sections to provide a comprehensive overview of experimental topics that were expanded upon as future directions informed by the data presented in **Chapter 2**. These subdivisions are organized as follows: (i) striatal mechanisms in AS model mice that may contribute to synaptic dysregulation, (ii) mechanisms of GABA co-release that may mediate motivational drive, and (iii) differing mechanisms of glutamate co-release that are unaffected with the loss of *Ube3a*.

3.1 Striatal mechanisms in AS model mice that may contribute to synaptic dysregulation

Ube3a$^{m-/p+}$ mice have been shown to be less affected by D2 antagonism mediated by raclopride administration (Riday et al., 2012) suggesting a potential mechanism underlying reward circuitry deficits. Raclopride similarly affects BSR threshold between AS and WT mice but lowers maximum response rate in AS model mice suggesting decreased D2-receptor function. While D2-receptor dysregulation

is a candidate within AS model mice, they respond to the same degree to D1-receptor antagonism as WT mice (Riday et al., 2012). D2-receptors are a $G_{i/o}$-coupled inhibitory auto-receptor that is associated with activation of the indirect pathway and acts to inhibit dopaminergic neuron excitability and attenuates DA release (**Section 1.2.3**; (Ford et al., 2006)). Given that D1- and D2-receptors are located both pre- and post-synaptically, the hyper-motivation phenotype observed within *Ube3a*$^{FLOX/p+}$ mice could potentially arise from a similar mechanism as suggested in the AS model mice. Using a real-time place preference (RTPP) paradigm, we coupled i.p. administration of raclopride along with optogenetic stimulation in *TH*^{CRE}::*Ube3a*$^{FLOX/p+}$ to determine if D2-receptors are similarly affected and in AS model mice when *Ube3a* is eliminated pre-synaptically in TH-expressing VTA neurons. Using 30 Hz stimulation, there was a trend for a decrease in sensitivity to D2-antagonism mediated by raclopride in *TH*^{CRE}::*Ube3a*$^{FLOX/p+}$ suggesting that *Ube3a* may regulate D2-receptor expression levels pre-synaptically that could lead to the observed hypermotivation (**Fig. 3.1**, p=0.059). However, this is unlikely given that engineered mice that are deficient for D2-receptors exhibit an increase in BSR threshold whereas AS model mice exhibit a decrease in threshold for BSR and for optogenetic VTA-to-NAc stimulation (Elmer et al., 2005; Riday et al., 2012). In addition, deletion of *Ube3a* within TH-expressing VTA neurons leads to no change in DA release providing further evidence that the mechanism underlying enhanced reward-seeking is not directly mediated by D2-receptor dysregulation. Moreover, D2-receptor protein expression is similar in AS model mice compared to wildtype mice suggesting that the insensitivity to D2 antagonism is not mediated by a

change in total D2 expression but rather D2-receptor function (data not shown). However, these data do provide some insight into where *Ube3a* expression is required (TH^+ neurons in the VTA) and how *Ube3a* may affect pre-synaptic transmission (GABA co-release deficient).

3.2 Mechanisms of GABA co-release and mechanisms that may mediate motivational drive

Dale's principle states that a neuron can only release one type of neurotransmitter regardless of its efferent projections. However, it has recently been identified that neurons are capable of releasing several types of neurotransmitters and neuropeptides. Specifically, mesolimbic dopaminergic neurons are capable of releasing glutamate, GABA, and dopamine in concert (Adrover et al., 2014; Hnasko and Edwards, 2012; Stuber et al., 2010; Tritsch et al., 2012; Tritsch et al., 2014). In 2012, it was first identified that dopaminergic neurons within the SNc can co-release GABA within the dorsal striatum (Tritsch et al., 2012). The mechanism underlying this co-release was mediated by GABA vesicular loading through the vesicular monoamine transporter (VMAT2) and is independent of VGAT. This finding was further expanded upon in 2014 with the establishment that GABA and DA co-release also occurs in dopaminergic neurons projecting to the ventral striatum (Tritsch et al., 2014). The mechanisms underlying this phenomenon largely remain unclear but it has been revealed that these dopaminergic neurons release GABA in a non-canonical manner mediated by VMAT2. DAergic terminals uptake ambient

GABA via membrane transporters GAT1 and VMAT2 and do not express any GABA synthetic enzymes (GAD65 and GAD67) contrary to previous reports suggesting that approximately 10% of VTA dopaminergic neurons express GAD65 (Tritsch et al., 2014). Because of this mechanism, repeated stimulation of these terminals in quick succession leads to oIPSC rundown which is an attribute of these synapses that needs to be taken under consideration with experimental design.

These known mechanisms lead to the hypothesis, along with the deficient GABA co-release observed upon *Ube3a* deletion in TH^+ neurons, that perhaps *Ube3a* is required for proper GABA uptake. To test this hypothesis, we utilized a CRE-dependent viral approach in which we exogenously introduced VGAT within the same neurons that are deficient for *Ube3a*. This will test if exogenous VGAT expression is sufficient to (1) rescue enhanced reward-seeking and (2) normalize GABA co-release physiologically. With this approach, we injected 500 nL of a 1:1 ratio of DIO-ChR2-EYFP along with DIO-VGAT in $TH^{CRE}::Ube3a^{FLOX/+}$ and $TH^{CRE}::Ube3a^{m+/p+}$ bilaterally within the VTA. Chronic optical fibers were implanted within the NAc as described in **section 2.5.1** to specifically target those terminals during a behavioral task. Animals then performed the optical ICSS behavioral task at a FR1 reinforcement schedule that delivered 30 Hz optical stimulation. Exogenous expression of VGAT within $TH^{CRE}::Ube3a^{FLOX/+}$::DIO-VGAT animals was found to be sufficient to rescue the hyper-motivational phenotype previously observed (**Fig. 3.2a**). While the rescue of motivational drive provided correlative evidence that enhancing GABA co-release within VTA terminals was sufficient, it

remained unclear if these terminals were then physiologically capable of reinstating concomitant GABA transmission as *TH^{CRE}::Ube3a$^{m+/p+}$*::DIO-VGAT.

To test this hypothesis, we interrogated this system to ask if GABA co-release within *TH^{CRE}::Ube3a$^{FLOX/+}$*::DIO-VGAT elevated to wild-type levels using *in vitro* whole-cell electrophysiology. Using an optical stimulation paradigm of 1-pulse and 30 Hz, there was not a statistical difference in GABA co-release between the two genotypes suggesting that extracellular available GABA concentration between *Ube3a$^{m+/p+}$* and *Ube3a$^{FLOX/p+}$* are similar but that *TH^{CRE}::Ube3a$^{FLOX/p+}$* mice exhibit deficient GABA uptake (**Fig. 3.2b**). These data provide novel correlative evidence for the involvement of GABA co-release from dopaminergic terminals in reward-seeking behavior. Currently, we are limited by the technology available to test the behavioral consequence of GABA co-release. An interesting future direction to test a true causal relationship within a wild-type mouse would be to delete mGAT1 in a cell type-specific manner within DAergic neurons in the VTA and test if this leads to an increase in motivation.

3.3 Glutamate co-release is unaffected with cell type-specific deletion of *Ube3a*.

As mentioned in section **3.2**, dopaminergic terminals are capable or releasing glutamate, GABA, and dopamine simultaneously. The mechanisms underlying these release events are beginning to come to light and are known to occur in two very distinct manners. GABA and DA are evidenced to be present within the same

synaptic vesicles and are uploaded by VMAT2 (Tritsch et al., 2012; Tritsch et al., 2014). GABA synthase is not present within DAergic neurons, but GABA is acquired from the synaptic cleft and is actively transported via GAT1 (Tritsch et al., 2014). However, recently the Morales group has shown that glutamate is not co-released in the same manner as GABA (Zhang et al., 2015) but occur in separate microdomains within the same terminal. Furthermore, the mechanism underlying vesicular loading of glutamate is mediated by VLGUT2 and not VMAT2 as suggested for GABA co-release (Tritsch et al., 2012; Zhang et al., 2015). To test if glutamate co-release is affected upon TH^{CRE} specific deletion of *Ube3a*, we injected DIO-ChR2-EYFP into TH^{CRE}*::Ube3a*$^{m+/p+}$ and TH^{CRE}*::Ube3a*$^{FLOX/p+}$ mice and used a 1-pulse optical stimulation paradigm as described in section **3.2**. We blocked all inhibitory synaptic transmission by placing picrotoxin (50 μM) in the recording solution to pharmacologically isolate excitatory events. We saw no statistically significant change in glutamate co-release between TH^{CRE}*::Ube3a*$^{m+/p+}$ and TH^{CRE}*::Ube3a*$^{FLOX/p+}$ mice suggesting that GABA co-release is uniquely affected by the loss of *Ube3a* (**Fig. 3.3**) and that VGLUT2-mediated synaptic vesicle loading is also unaffected.

3.5 Materials and Methods

3.5.1 Experimental Subjects and Stereotaxic Surgeries

Cg-Tg-TH:Cre mice (008601) were obtained through Jackson Laboratories. *Ube3a-floxed* mice were engineered by Matthew Judson in conjunction with the UNC Animal Models Core. These mice were on a C57/BL6 background except for the *Ube3a-floxed* mice which were mixed with a 129S6:C57BL/6 background but backcrossed eight generations before experimental use. Mice for electrophysiological recordings were aged P60-P90 and were compared to wild-type age and sex matched controls. The experimenter was blind to genotype and littermate controls were used when possible. Behavioral mice were group housed until surgery and were taken at 25-30g. We anesthetized the mice with ketamine (150mg/kg) and xylazine (50mg/kg) and placed the mice in a stereotaxic frame (Kopf Instruments). We bilaterally microinjected 0.5µL of purified adeno-associated virus (~10^{12} infections units per ml, packaged and tittered by the UNC Viral Vector Core Facility) into the VTA (coordinates from bregma: -3.15 anterior/posterior, ±0.75 medial/lateral, -4.75 dorsal/ventral). VTA neurons in TH^{Cre} positive $Ube3a^{m-/p+}$, $Ube3a^{FLOX/+}$, or $Ube3a^{m+/p+}$ mice were trasnsduced with virus encoding ChR2-eYFP under the control of the human synapsin (*SYN1*) promoter along with VGAT (generously provided by Bernardo Sabatini). Following surgery, mice were individually housed. For behavioral experiments, we also implanted mice with bilateral chronic fiber directed above the NAc (coordinates from bregma: +1.2 A/P,

±1.6 M/L, -4.6 D/V at a 10°angle). We performed all experiments 5-8 weeks after surgery. We conducted all procedures in accordance with the Guide for the Care and Use of Laboratory Animals as adopted by the National Institutes of Health, and with approval of the UNC Institutional Animal Care and Use committees.

3.5.2 *In vivo* optogenetic excitation

For all behavioral experiments, mice were injected with AAV5-EF1α-DIO-ChR2-eYFP virus and implanted with bilateral custom-made optical fiber targeted to the NAc core (Sparta et al., 2012). Mice were connected to a 'dummy' optical patch cable 5 days before the experiment each day for 60 min to habituate them to the tether procedure. Following the tethering procedure, we ran the mice in several behavioral procedures (detailed below). We used a 10 mW, 473 nm laser with a stimulation frequency of 30 Hz and a 5 ms pulse width duration for all behavioral assays unless otherwise noted.

3.5.3 Real-time Place Preference

We placed mice in a behavioral arena (50 x 50 x 25 cm black) for 20 min. One (counterbalanced) side of the camber was assigned as the stimulation side. The mouse was placed in the nonstimulated side at the onset of the experiment and delivered a 5, 10, 20, 30, 40, or 60 Hz (randomized) constant laser stimulation each time the mouse crossed to the stimulation side of the chamber until the mouse crossed back into the nonstimulation side. We recorded behavioral data via a CCD

camera interfaced with Ethovision XT software (Noldus Information Technologies). Mice underwent one session per day.

In vivo pharmacology: After mice completed the RTPP task, they were administered i.p. with raclopride (0.1 mg/kg), SCH23390 (0.06 mg/kg), or saline (counterbalanced between days). All drugs were dissolved in 0.9% sterile saline. Mice were allowed to recover post-injection for 20 min in their home cage. Following recovery, mice were run through the RTPP task as described above except received a single frequency (30 Hz) stimulation. Mice had at least 24 hours without manipulation between each i.p. drug administration.

3.5.4 Voltage-clamp Recordings

In vitro optogenetic stimulation of GABA co-release was performed in the same manner as stated in section **2.5.3**. Briefly, 250 µM coronally prepared striatal sections were placed in a bath containing AMPA and NMDA receptor blockers or picrotoxin then stimulated with either 1, 20 ms optical pulse or a 1 s train at 30 Hz.

3.5.5 Positive reinforcement procedures and Optical Self-Stimulation

Behavioral training and testing occurred in mouse operant chambers (Med Associates) interfaced with optogenetic stimulation equipment. Behavioral paradigms were performed during their respective dark cycle. Food restricted male mice (90% of their free-feeding bodyweight) were trained on a fixed ratio (1:1) training schedule for one session per day for 60 min, in which each nose poke resulted in 20 µl of a 15% sucrose administration until the number of nose pokes did

not vary >20% across three consecutive days. In addition, active nose poke ports were coupled with a cue light that remained on. With each successful nose poke, the cue light turned off and a tone would be presented for 3 s. Once the mice reached a stable number of nose pokes, they were habituated for 5 consecutive days to the patch cable with optical stimulation (3 s of 30 Hz) time-locked to the cue following each active nose poke. After the 5 day habituation phase, mice were then tested following a 2 day break. Active and inactive nose pokes were recorded in addition to time-stamps.

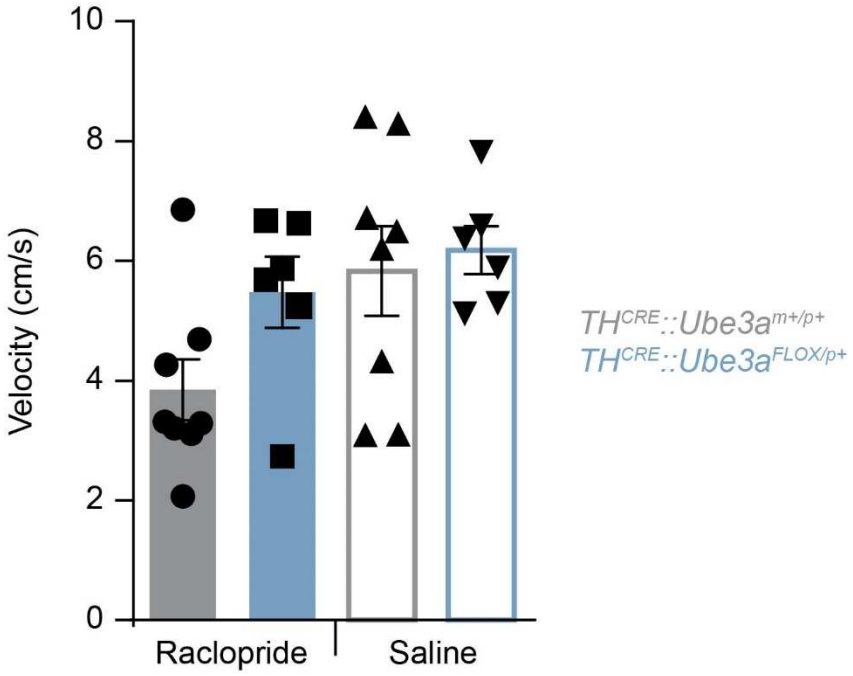

Figure 3.1: Cell type-specific deletion of *Ube3a* in TH⁺ neurons may lead to insensitivity to D2-antagonism.

Mice were placed in a real-time place-preference arena after being injected with raclopride (0.1 mg/kg) 20 min prior to behavioral testing. Mean velocity was then measured across an entire 20 minute session. While there is no statistically significant difference (p=0.59), there is a trend suggesting that *TH^{CRE}::Ube3a$^{FLOX/p+}$* mice may be insensitive to D2 antagonism mediated by raclopride that should be investigated further (n=8 and 6). Bars represent mean ± SEM.

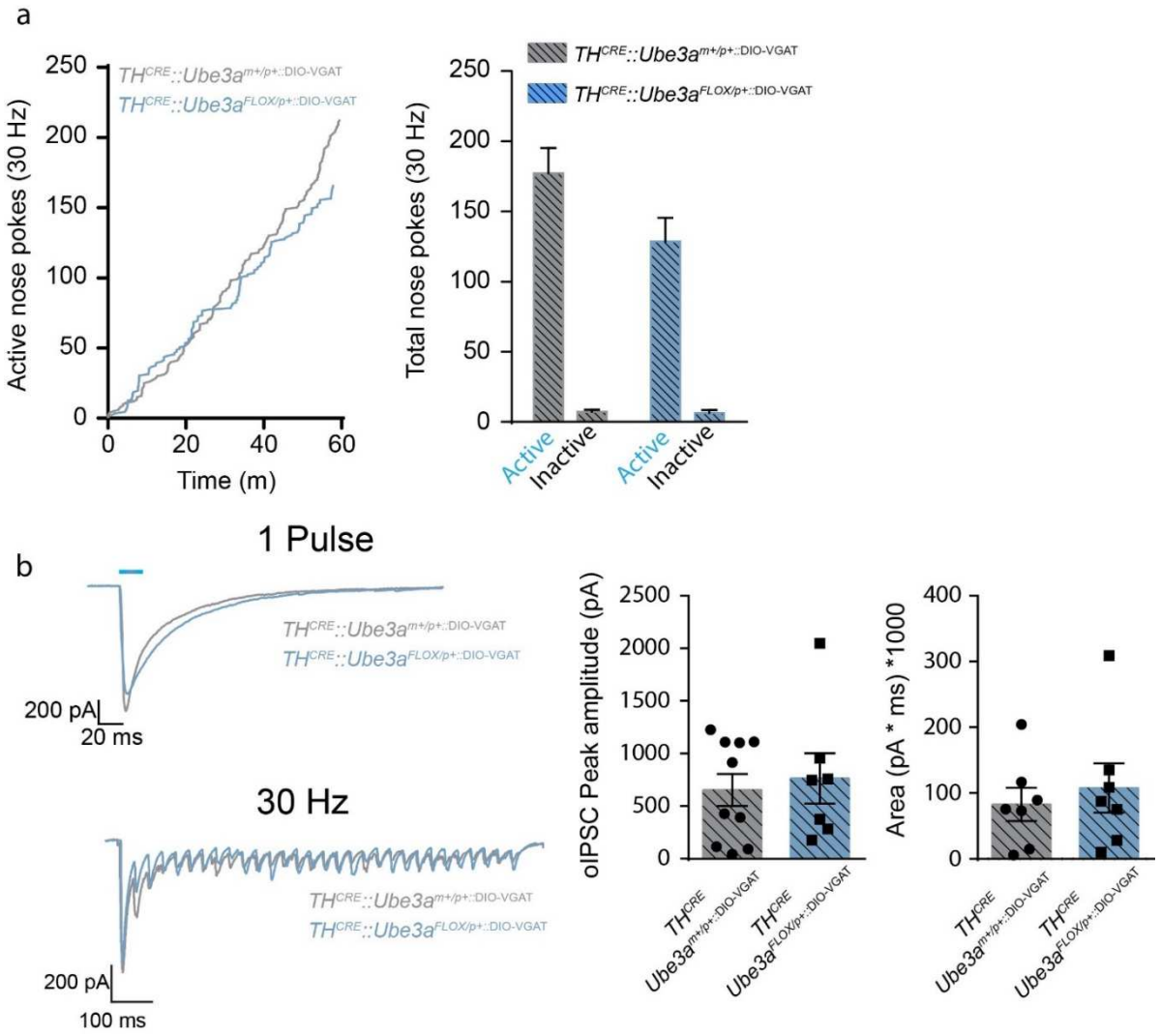
a
Active nose pokes (30 Hz)
Time (m)
THCRE::Ube3am+/p+::DIO-VGAT
THCRE::Ube3aFLOX/p+::DIO-VGAT
Total nose pokes (30 Hz)
Active
Inactive
b
1 Pulse
200 pA
20 ms
30 Hz
100 ms
oIPSC Peak amplitude (pA)
Area (pA * ms) *1000

Figure 3.2: Exogenous expression of VGAT in TH^{+} cells ameliorates enhanced reward-seeking and normalizes GABA co-release in *TH^{CRE}::Ube3a$^{FLOX/p+}$* mice.

(**a**) Left: Cumulative response plots showing cumulative nose pokes that trigger a 30 Hz, 473 nm stimulus (active nose pokes) in representative mice. Right: Average number of nose pokes for triggering (active nose pokes) or not triggering (inactive) 30 Hz optical stimulation across a 60 minute session. *TH^{CRE}::Ube3a$^{m+/p+}$*::DIO-VGAT and *TH^{CRE}::Ube3a$^{FLOX/p+}$*::DIO-VGAT mice poked at similar levels for self-stimulation in the presence of VGAT expression (n=5, 4; p=0.06). (**b**) Left: Representative oIPSC traces measured in *TH^{CRE}::Ube3a$^{FLOX/p+}$*::DIO-VGAT and *TH^{CRE}::Ube3a$^{m+/p+}$*::DIO-VGAT mice and evoked by single pulses (20 ms) or 30 Hz trains of stimulation. The pharmacological isolation of GABAergic currents was validated by application of the antagonist SR95531. Center: Average peak amplitude of single oIPSCs demonstrate similar GABAergic currents in *Ube3a$^{FLOX/p+}$*::DIO-VGAT mice when compared to controls (n=10 and 7, p=0.689). Right: Average oIPSC charge evoked using a similar 30 Hz optical stimulation paradigm employed behaviorally and tested *in vitro* (n= 7 and 7, p=0.589). Bars represent mean ± SEM.

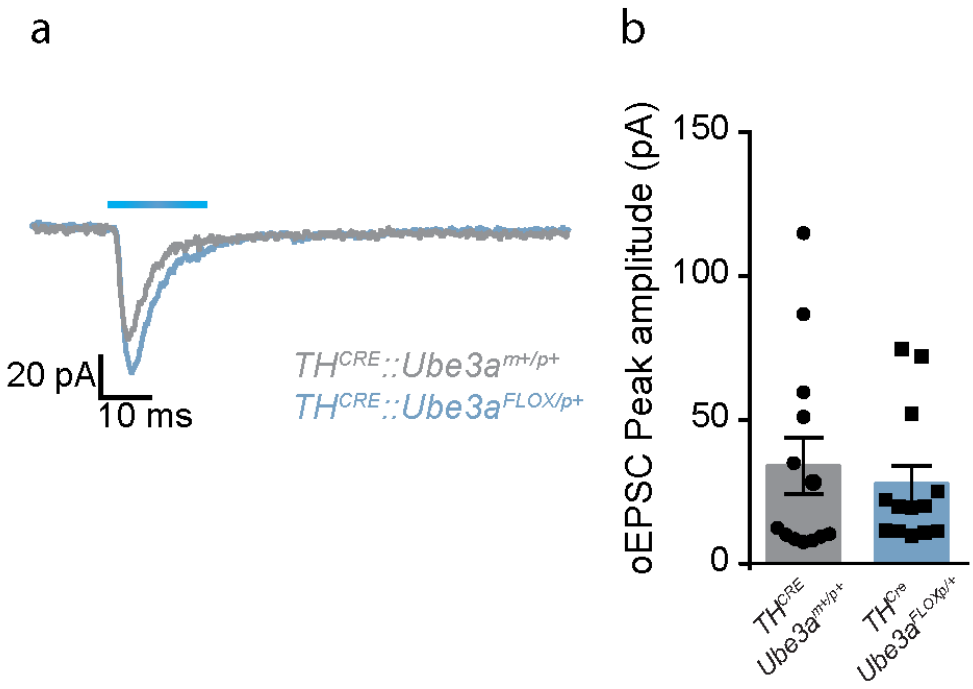

Figure 3.3: Glutamate co-release is similar between *TH^{CRE}::Ube3a$^{m+/p+}$* and *TH^{CRE}::Ube3a$^{FLOX/p+}$* mice. (**a**) Representative averaged traces (≥ 6 sweeps) of glutamate co-release from TH-expressing VTA-to-NAc terminals. (**b**) Average peak amplitude of single oEPSCs demonstrate similar excitatory currents in *TH^{CRE}::Ube3a$^{m+/p+}$* and *TH^{CRE}::Ube3a$^{FLOX/p+}$* mice (n=13/genotype, p=0.59). All bars represent mean ± SEM.

CHAPTER 4

DISCUSSION

The following chapter is subdivided into two main sections that are composed of avenues that could be pursued guided by the data presented in chapters 2 and 3. The first subdivision discusses (ii) upstream pathways that could contribute to circuit dysfunction, and the second discusses (ii) molecular constituents in AS model mice that may contribute to disrupted GABA co-release which may be potential neuronal substrates of UBE3A.

4.1 Upstream pathways that could contribute to circuit dysfunction

As described in section **1.2.3**, there are several additional anatomical targets upstream of the VTA that are essential to appetitive behaviors such as the dorsal striatum and mPFC. Mice develop a strong preference for optical stimulation of the VTA-to-NAc pathway that may be exclusively regulated exclusively by GABA co-release. However, this does not take into account mPFC and dorsal striatum mediated higher order processes also play an important regulatory role in motivation and reward-seeking. An additional aspect to consider is that these mPFC and

striatal targets reciprocally target the VTA providing bidirectional feedback to the VTA (Kauer and Malenka, 2007). DA release from the VTA during a rewarding stimulus results in post-synaptic neurons expressing a form of NMDAR-dependent LTP that increases AMPA/NMDA ratio (Kauer and Malenka, 2007) in order to make an association more salient. Because of these additional VTA targets and their reciprocal connections, an interesting future direction would be to assess the plasticity induced within the striatum in *TH^{CRE}::Ube3a$^{FLOX/p+}$* and *TH^{CRE}::Ube3a$^{m+/p+}$* mice and how they may differ after optical self-stimulation. In addition, it will be necessary to interrogate several parts of the circuit and assay if VTA-to-striatum-to-mPFC connections mediate the same hyper-motivational phenotypes as VTA-to-NAc as well as VTA-to-dorsal striatum.

In addition, the mPFC has been highlighted for its important role in behavioral extinction during extinction of reward-seeking and fear-conditioning (Kim et al., 2009; Milad and Quirk, 2002; Sparta et al., 2014). Recently, *in vivo* optogenetic manipulations of parvalbumin-containing fast spiking interneurons (PV$^+$ FSIs) has shown that activation of PV$^+$ FSI accelerates extinction of a reward-seeking paradigm (Sparta et al., 2014). Given that AS model mice are known to have deficits in inhibitory transmission (Wallace et al., 2012) and GABA co-release from TH$^+$ neurons (**Chapter 2**), an intriguing future direction would be to test extinction of a reward-seeking paradigm in AS model mice. If there are differences, testing if this change coincides with aberrant inhibitory drive in the PFC would be of interest.

The Philpot lab has acquired preliminary, unpublished data suggesting that instrumental extinction is enhanced in AS model mice as in Fmr1 knockout mice

(Sidorov et al., 2014). Considering the robust role the mPFC has in working memory (Seamans and Yang, 2004), which facilitates the acquisition of reinforcing behaviors, the mPFC will be an important anatomical target to study in *TH^{CRE}::Ube3a$^{FLOX/p+}$* mice. The mPFC receives dopaminergic input from the VTA (Kauer and Malenka, 2007), and in conjunction with the behavioral extinction data, provides an anatomical substrate to consider in AS circuitry. An interesting electrophysiological property to test would be if the dopaminergic inputs to the mPFC also co-release GABA and if so, if this is altered in *TH^{CRE}::Ube3a$^{FLOX/p+}$* mice. In addition, PV^{+} FSIs have an important role in modulating extinction. The use of genetic tools (PV-specific CRE) would be necessary to test using selective *Ube3a* deletion in PV^{+} interneurons. As mentioned above, the use optogenetics has elucidated an important role for FSI in extinction. The characterized excitatory-inhibitory imbalance within AS model mice would suggest a hyperexcitability due to a decrease in inhibition (Wallace et al., 2012). Because AS mice are thought to have enhanced instrumental extinction, an interesting future direction would be to delete *Ube3a* in PV^{+} FSI and test if the loss of *Ube3a* specifically within these neurons alters instrumental extinction.

4.2 Molecular constituents in AS model mice that may contribute to disrupted GABA co-release

GAT1 has been proposed as a potential UBE3A substrate within cerebellar granule cells (Egawa et al., 2012). Loss of UBE3A results in an increase in GAT1 expression which depletes available ambient GABA in the extra-synaptic cleft leading to a decrease in tonic inhibition. Further evidence for GAT1 as a molecular substrate lies in biochemical evidence analyzing cerebellar protein lysates from both *Ube3a*$^{m-/p+}$ and *Ube3a*$^{m+/p+}$ mice that suggests loss of *Ube3a* results in increased GAT1 expression (Egawa et al., 2012). These results provide convincing evidence for GAT1 as a potential neuronal substrate for UBE3A and is suggestive of *hyper*-functional GABA reuptake. Within UBE3A-null VTA terminals, this seems like an unlikely mechanism for the observed decrease in GABA co-release. If GAT1 were upregulated within VTA-to-NAc terminals, this would suggest a possible *increase* in GABA co-release that would theoretically be at a ceiling that would not be affected by VGAT expression. Considering that the exogenous viral expression of VGAT within TH$^+$ terminals leads to an increase in GABA co-release and, a rescue in reward-seeking behavior, it is unlikely that GAT1 is hyper-functional within this anatomical region within UBE3A-deficient neurons. However, GAT1 would mediate GABA reuptake and is not directly related to vesicular loading of GABA. There is a possibility that UBE3A may have a role in regulating GABA vesicular loading within these terminals leading to dysfunctional concomitant GABA release in dopaminergic terminals. While this is a probable hypothesis, cortical VGAT expression within *Ube3a*-deficient mice is similar to wild-type mice (Wallace et al.,

2012) but there is a marked increase in clathrin coated vesicles that suggests defective vesicle recycling. While it is not clear how the loss of *Ube3a* leads to a decrease in inhibitory transmission, candidates that should be considered for future studies include VGAT, VMAT2, and GAT1 in addition to vesicular docking proteins like synaptojanin or endophilin in VTA terminals (Cremona et al., 1999; Milosevic et al., 2011; Wallace et al., 2012).

More convincingly, GAT1 and GAT4 are the two GABA transporters that have been shown to be the source of GABA uptake for DAergic terminals in the VTA (Tritsch et al., 2014). Tritsch and colleagues have shown that VTA DAergic neurons do not express GABA synthase (*Gad65/67*) but, actively use GAT1/4 to uptake GABA from the extrasynaptic cleft. The data presented in **chapters 2** and **3,** along with the proposal of GAT1 as a UBE3A substrate, provide convincing evidence that UBE3A may, in fact, regulate GAT1 function leading to dysfunctional GABA co-release (**Fig. 4.1**). Given this possibility, a future direction of interest would be to perform a combinatorial approach of cell type-specific labeling in $TH^{CRE}::Ube3a^{FLOX/p+}$ mice along with ultrastructual imaging (e.g. electron microscopy) to determine if GAT1 expression is changed upon loss of *Ube3a*. In addition, we have shown that cell type-specific exogenous expression can ameliorate the hypermotivational phenotype observed in $TH^{CRE}::Ube3a^{FLOX/p+}$ mice. Therefore, it would be constructive to test if exogenous expression of GAT1 within these same neurons can rescue hypermotivation and GABA co-release upon *Ube3a* deletion in TH^+ neurons or if cell type-specific deletion of GAT1 within TH^+ neurons in wildtype mice phenocopy $TH^{CRE}::Ube3a^{FLOX/p+}$ mice.

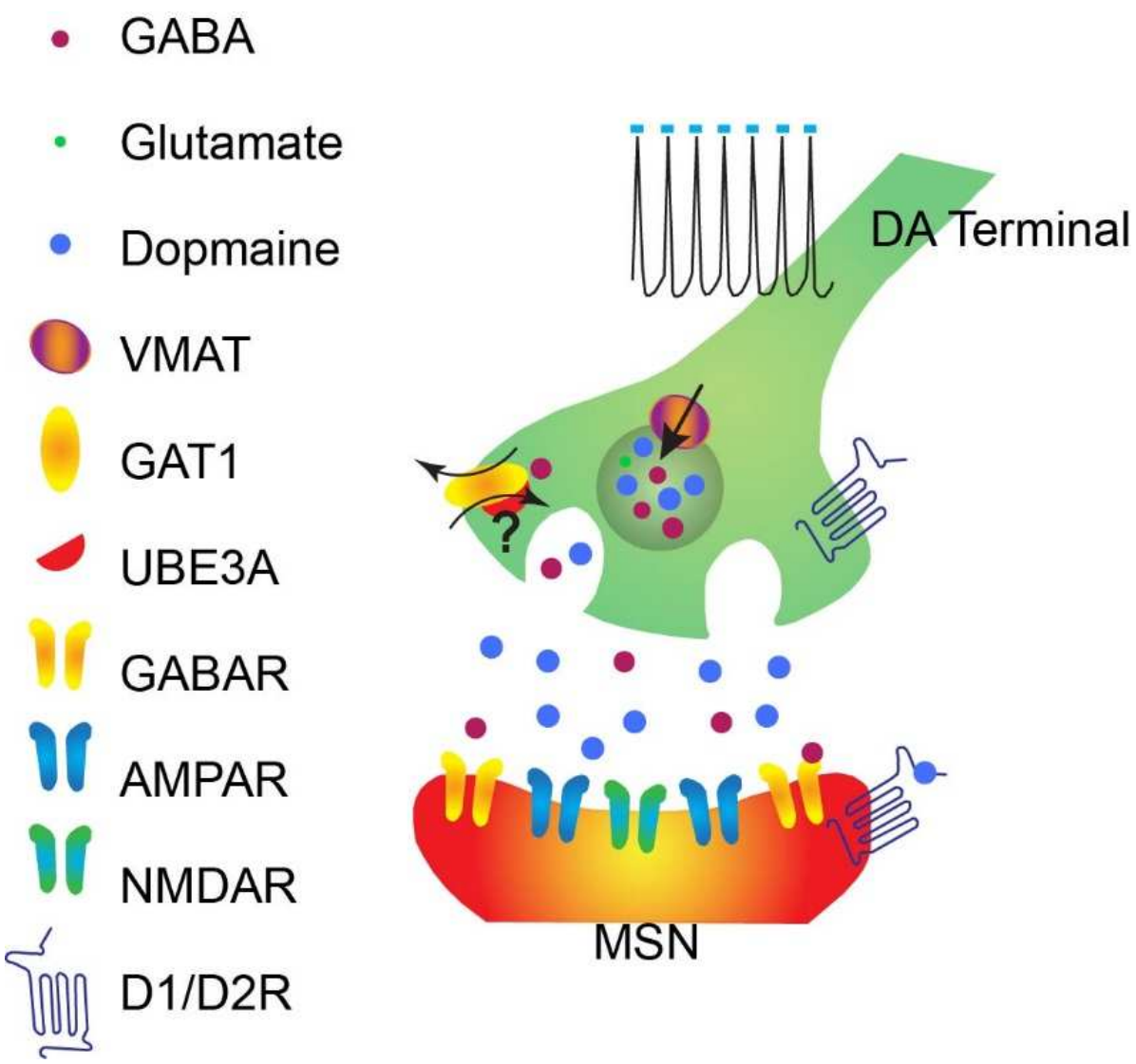
GABA
Glutamate
Dopmaine
VMAT
GAT1
UBE3A
GABAR
AMPAR
NMDAR
D1/D2R
DA Terminal
?
MSN

Figure 4.1: A proposed synaptic model within the nucleus accumbens.

A dopaminergic terminal (green) and medium spiny neuron terminal (red) are represented along with the key components that have been informed by the data presented in this thesis. A synaptic vesicle is shown that contains three different neurotransmitters dopamine, glutamate and GABA that are being released by the optically driven ChR2 leading to action potential generation. VMAT fluxes in these neurotransmitters into the synaptic vesicle to package them for future membrane docking and release. GAT1 is a membrane bound transporter that imports GABA into a dopaminergic terminal and is illustrated as a bidirectional process by the arrows. UBE3A is represented as possibly being associated with GAT1 as a proposed substrate to facilitate GABA influx. Loss of UBE3A may lead to attentuated GABA influx leading to the decrease of GABA co-release observed in $TH^{CRE}::UBE3A^{FLOX/p+}$ mice. Action potentials represented in the DAergic terminal are optogenetically driven to specifically drive these terminals to gain the ability to observe these co-release phenomenon in the post-synaptic MSN.

REFERENCES

Adrover, M.F., Shin, J.H., and Alvarez, V.A. (2014). Glutamate and dopamine transmission from midbrain dopamine neurons share similar release properties but are differentially affected by cocaine. J Neurosci *34*, 3183-3192.

Angelman, H. (1965). Puppet Children - a Report on 3 Cases. Dev Med Child Neurol *7*, 681-&.

Bjorklund, A., and Dunnett, S.B. (2007). Dopamine neuron systems in the brain: an update. Trends Neurosci *30*, 194-202.

Bromberg-Martin, E.S., Matsumoto, M., and Hikosaka, O. (2010). Dopamine in motivational control: rewarding, aversive, and alerting. Neuron *68*, 815-834.

Clayton-Smith, J. (2003). Genomic imprinting as a cause of disease. BMJ *327*, 1121-1122.

Cooper, E.M., Hudson, A.W., Amos, J., Wagstaff, J., and Howley, P.M. (2004). Biochemical analysis of Angelman syndrome-associated mutations in the E3 ubiquitin ligase E6-associated protein. J Biol Chem *279*, 41208-41217.

Cremona, O., Di Paolo, G., Wenk, M.R., Luthi, A., Kim, W.T., Takei, K., Daniell, L., Nemoto, Y., Shears, S.B., Flavell, R.A.*, et al.* (1999). Essential role of phosphoinositide metabolism in synaptic vesicle recycling. Cell *99*, 179-188.

Dichter, G.S., Damiano, C.A., and Allen, J.A. (2012). Reward circuitry dysfunction in psychiatric and neurodevelopmental disorders and genetic syndromes: animal models and clinical findings. J Neurodev Disord *4*, 19.

Dindot, S.V., Antalffy, B.A., Bhattacharjee, M.B., and Beaudet, A.L. (2008). The Angelman syndrome ubiquitin ligase localizes to the synapse and nucleus, and maternal deficiency results in abnormal dendritic spine morphology. Hum Mol Genet *17*, 111-118.

Dolen, G., Darvishzadeh, A., Huang, K.W., and Malenka, R.C. (2013). Social reward requires coordinated activity of nucleus accumbens oxytocin and serotonin. Nature *501*, 179-184.

Dreyer, J.K., Herrik, K.F., Berg, R.W., and Hounsgaard, J.D. (2010). Influence of phasic and tonic dopamine release on receptor activation. J Neurosci *30*, 14273-14283.

Egawa, K., Kitagawa, K., Inoue, K., Takayama, M., Takayama, C., Saitoh, S., Kishino, T., Kitagawa, M., and Fukuda, A. (2012). Decreased tonic inhibition in

cerebellar granule cells causes motor dysfunction in a mouse model of Angelman syndrome. Sci Transl Med *4*, 163ra157.

Elmer, G.I., Pieper, J.O., Levy, J., Rubinstein, M., Low, M.J., Grandy, D.K., and Wise, R.A. (2005). Brain stimulation and morphine reward deficits in dopamine D2 receptor-deficient mice. Psychopharmacology (Berl) *182*, 33-44.

Farook, M.F., DeCuypere, M., Hyland, K., Takumi, T., LeDoux, M.S., and Reiter, L.T. (2012). Altered serotonin, dopamine and norepinepherine levels in 15q duplication and Angelman syndrome mouse models. PLoS One *7*, e43030.

Ferdousy, F., Bodeen, W., Summers, K., Doherty, O., Wright, O., Elsisi, N., Hilliard, G., O'Donnell, J.M., and Reiter, L.T. (2011). Drosophila Ube3a regulates monoamine synthesis by increasing GTP cyclohydrolase I activity via a non-ubiquitin ligase mechanism. Neurobiol Dis *41*, 669-677.

Fields, H.L., and Margolis, E.B. (2015). Understanding opioid reward. Trends Neurosci *38*, 217-225.

Floresco, S.B. (2015). The nucleus accumbens: an interface between cognition, emotion, and action. Annu Rev Psychol *66*, 25-52.

Ford, C.P., Mark, G.P., and Williams, J.T. (2006). Properties and opioid inhibition of mesolimbic dopamine neurons vary according to target location. J Neurosci *26*, 2788-2797.

Frank, M.J. (2005). Dynamic dopamine modulation in the basal ganglia: a neurocomputational account of cognitive deficits in medicated and nonmedicated Parkinsonism. J Cogn Neurosci *17*, 51-72.

Gantz, S.C., Ford, C.P., Neve, K.A., and Williams, J.T. (2011). Loss of Mecp2 in substantia nigra dopamine neurons compromises the nigrostriatal pathway. J Neurosci *31*, 12629-12637.

Geschwind, D.H., and Levitt, P. (2007). Autism spectrum disorders: developmental disconnection syndromes. Curr Opin Neurobiol *17*, 103-111.

Grace, A.A. (1991). Regulation of spontaneous activity and oscillatory spike firing in rat midbrain dopamine neurons recorded in vitro. Synapse *7*, 221-234.

Grace, A.A., Floresco, S.B., Goto, Y., and Lodge, D.J. (2007). Regulation of firing of dopaminergic neurons and control of goal-directed behaviors. Trends Neurosci *30*, 220-227.

Grace, A.A., and Onn, S.P. (1989). Morphology and electrophysiological properties of immunocytochemically identified rat dopamine neurons recorded in vitro. J Neurosci *9*, 3463-3481.

Hamilton, P.J., Campbell, N.G., Sharma, S., Erreger, K., Herborg Hansen, F., Saunders, C., Belovich, A.N., Consortium, N.A.A.S., Sahai, M.A., Cook, E.H., *et al.* (2013). De novo mutation in the dopamine transporter gene associates dopamine dysfunction with autism spectrum disorder. Mol Psychiatry *18*, 1315-1323.

Harbord, M. (2001). Levodopa responsive Parkinsonism in adults with Angelman Syndrome. J Clin Neurosci *8*, 421-422.

Hnasko, T.S., and Edwards, R.H. (2012). Neurotransmitter corelease: mechanism and physiological role. Annu Rev Physiol *74*, 225-243.

Huang, H.S., Burns, A.J., Nonneman, R.J., Baker, L.K., Riddick, N.V., Nikolova, V.D., Riday, T.T., Yashiro, K., Philpot, B.D., and Moy, S.S. (2013). Behavioral deficits in an Angelman syndrome model: effects of genetic background and age. Behav Brain Res *243*, 79-90.

Huys, Q.J., Daw, N.D., and Dayan, P. (2015). Depression: A Decision-Theoretic Analysis. Annu Rev Neurosci *38*, 1-23.

Jiang, Y.H., Armstrong, D., Albrecht, U., Atkins, C.M., Noebels, J.L., Eichele, G., Sweatt, J.D., and Beaudet, A.L. (1998). Mutation of the Angelman ubiquitin ligase in mice causes increased cytoplasmic p53 and deficits of contextual learning and long-term potentiation. Neuron *21*, 799-811.

Jones, S.R., O'Dell, S.J., Marshall, J.F., and Wightman, R.M. (1996). Functional and anatomical evidence for different dopamine dynamics in the core and shell of the nucleus accumbens in slices of rat brain. Synapse *23*, 224-231.

Kaphzan, H., Buffington, S.A., Jung, J.I., Rasband, M.N., and Klann, E. (2011). Alterations in intrinsic membrane properties and the axon initial segment in a mouse model of Angelman syndrome. J Neurosci *31*, 17637-17648.

Kauer, J.A., and Malenka, R.C. (2007). Synaptic plasticity and addiction. Nat Rev Neurosci *8*, 844-858.

Keeler, J.F., Pretsell, D.O., and Robbins, T.W. (2014). Functional implications of dopamine D1 vs. D2 receptors: A 'prepare and select' model of the striatal direct vs. indirect pathways. Neuroscience *282C*, 156-175.

Kim, J.H., Hamlin, A.S., and Richardson, R. (2009). Fear extinction across development: the involvement of the medial prefrontal cortex as assessed by temporary inactivation and immunohistochemistry. J Neurosci *29*, 10802-10808.

Lammel, S., Hetzel, A., Hackel, O., Jones, I., Liss, B., and Roeper, J. (2008). Unique properties of mesoprefrontal neurons within a dual mesocorticolimbic dopamine system. Neuron *57*, 760-773.

Lammel, S., Ion, D.I., Roeper, J., and Malenka, R.C. (2011). Projection-specific modulation of dopamine neuron synapses by aversive and rewarding stimuli. Neuron *70*, 855-862.

Lammel, S., Lim, B.K., and Malenka, R.C. (2014). Reward and aversion in a heterogeneous midbrain dopamine system. Neuropharmacology *76 Pt B*, 351-359.

Lammel, S., Steinberg, E.E., Foldy, C., Wall, N.R., Beier, K., Luo, L., and Malenka, R.C. (2015). Diversity of transgenic mouse models for selective targeting of midbrain dopamine neurons. Neuron *85*, 429-438.

Landers, M., Calciano, M.A., Colosi, D., Glatt-Deeley, H., Wagstaff, J., and Lalande, M. (2005). Maternal disruption of Ube3a leads to increased expression of Ube3a-ATS in trans. Nucleic Acids Res *33*, 3976-3984.

Larsen, R.S., Smith, I.T., Miriyala, J., Han, J.E., Corlew, R.J., Smith, S.L., and Philpot, B.D. (2014). Synapse-specific control of experience-dependent plasticity by presynaptic NMDA receptors. Neuron *83*, 879-893.

Laurent, V., and Balleine, B.W. (2015). Factual and Counterfactual Action-Outcome Mappings Control Choice between Goal-Directed Actions in Rats. Curr Biol *25*, 1074-1079.

Mabb, A.M., Judson, M.C., Zylka, M.J., and Philpot, B.D. (2011). Angelman syndrome: insights into genomic imprinting and neurodevelopmental phenotypes. Trends Neurosci *34*, 293-303.

Margolis, E.B., Lock, H., Hjelmstad, G.O., and Fields, H.L. (2006). The ventral tegmental area revisited: is there an electrophysiological marker for dopaminergic neurons? J Physiol *577*, 907-924.

Martinez-Noel, G., Galligan, J.T., Sowa, M.E., Arndt, V., Overton, T.M., Harper, J.W., and Howley, P.M. (2012). Identification and proteomic analysis of distinct UBE3A/E6AP protein complexes. Mol Cell Biol *32*, 3095-3106.

Matsuura, T., Sutcliffe, J.S., Fang, P., Galjaard, R.J., Jiang, Y.H., Benton, C.S., Rommens, J.M., and Beaudet, A.L. (1997). De novo truncating mutations in E6-AP ubiquitin-protein ligase gene (UBE3A) in Angelman syndrome. Nat Genet *15*, 74-77.

McCarthy, S.E., Makarov, V., Kirov, G., Addington, A.M., McClellan, J., Yoon, S., Perkins, D.O., Dickel, D.E., Kusenda, M., Krastoshevsky, O.*, et al.* (2009). Microduplications of 16p11.2 are associated with schizophrenia. Nat Genet *41*, 1223-1227.

Milad, M.R., and Quirk, G.J. (2002). Neurons in medial prefrontal cortex signal memory for fear extinction. Nature *420*, 70-74.

Milosevic, I., Giovedi, S., Lou, X., Raimondi, A., Collesi, C., Shen, H., Paradise, S., O'Toole, E., Ferguson, S., Cremona, O.*, et al.* (2011). Recruitment of endophilin to

clathrin-coated pit necks is required for efficient vesicle uncoating after fission. Neuron *72*, 587-601.

Montague, P.R., Dayan, P., and Sejnowski, T.J. (1996). A framework for mesencephalic dopamine systems based on predictive Hebbian learning. J Neurosci *16*, 1936-1947.

Mulherkar, S.A., and Jana, N.R. (2010). Loss of dopaminergic neurons and resulting behavioural deficits in mouse model of Angelman syndrome. Neurobiol Dis *40*, 586-592.

Nair-Roberts, R.G., Chatelain-Badie, S.D., Benson, E., White-Cooper, H., Bolam, J.P., and Ungless, M.A. (2008). Stereological estimates of dopaminergic, GABAergic and glutamatergic neurons in the ventral tegmental area, substantia nigra and retrorubral field in the rat. Neuroscience *152*, 1024-1031.

Nicholls, R.D., and Knepper, J.L. (2001). Genome organization, function, and imprinting in Prader-Willi and Angelman syndromes. Annu Rev Genomics Hum Genet *2*, 153-175.

Olds, J., and Milner, P. (1954). Positive reinforcement produced by electrical stimulation of septal area and other regions of rat brain. J Comp Physiol Psychol *47*, 419-427.

Ostlund, S.B., Wassum, K.M., Murphy, N.P., Balleine, B.W., and Maidment, N.T. (2011). Extracellular dopamine levels in striatal subregions track shifts in motivation and response cost during instrumental conditioning. J Neurosci *31*, 200-207.

Philpot, B.D., Espinosa, J.S., and Bear, M.F. (2003). Evidence for altered NMDA receptor function as a basis for metaplasticity in visual cortex. J Neurosci *23*, 5583-5588.

Portmann, T., Yang, M., Mao, R., Panagiotakos, G., Ellegood, J., Dolen, G., Bader, P.L., Grueter, B.A., Goold, C., Fisher, E.*, et al.* (2014). Behavioral abnormalities and circuit defects in the basal ganglia of a mouse model of 16p11.2 deletion syndrome. Cell Rep *7*, 1077-1092.

Rice, M.E., and Cragg, S.J. (2008). Dopamine spillover after quantal release: rethinking dopamine transmission in the nigrostriatal pathway. Brain Res Rev *58*, 303-313.

Riday, T.T., Dankoski, E.C., Krouse, M.C., Fish, E.W., Walsh, P.L., Han, J.E., Hodge, C.W., Wightman, R.M., Philpot, B.D., and Malanga, C.J. (2012). Pathway-specific dopaminergic deficits in a mouse model of Angelman syndrome. J Clin Invest *122*, 4544-4554.

Robinson, D.L., Venton, B.J., Heien, M.L., and Wightman, R.M. (2003). Detecting subsecond dopamine release with fast-scan cyclic voltammetry in vivo. Clin Chem *49*, 1763-1773.

Robinson, T.E., and Berridge, K.C. (1993). The neural basis of drug craving: an incentive-sensitization theory of addiction. Brain Res Brain Res Rev *18*, 247-291.

Robison, A.J., and Nestler, E.J. (2011). Transcriptional and epigenetic mechanisms of addiction. Nat Rev Neurosci *12*, 623-637.

Rothwell, P.E., Fuccillo, M.V., Maxeiner, S., Hayton, S.J., Gokce, O., Lim, B.K., Fowler, S.C., Malenka, R.C., and Sudhof, T.C. (2014). Autism-associated neuroligin-3 mutations commonly impair striatal circuits to boost repetitive behaviors. Cell *158*, 198-212.

Russo, S.J., and Nestler, E.J. (2013). The brain reward circuitry in mood disorders. Nat Rev Neurosci *14*, 609-625.

Samaco, R.C., Mandel-Brehm, C., Chao, H.T., Ward, C.S., Fyffe-Maricich, S.L., Ren, J., Hyland, K., Thaller, C., Maricich, S.M., Humphreys, P.*, et al.* (2009). Loss of MeCP2 in aminergic neurons causes cell-autonomous defects in neurotransmitter synthesis and specific behavioral abnormalities. Proc Natl Acad Sci U S A *106*, 21966-21971.

Sato, M., and Stryker, M.P. (2010). Genomic imprinting of experience-dependent cortical plasticity by the ubiquitin ligase gene Ube3a. Proc Natl Acad Sci U S A *107*, 5611-5616.

Sawaguchi, T., and Goldman-Rakic, P.S. (1994). The role of D1-dopamine receptor in working memory: local injections of dopamine antagonists into the prefrontal cortex of rhesus monkeys performing an oculomotor delayed-response task. J Neurophysiol *71*, 515-528.

Schultz, W. (1998). Predictive reward signal of dopamine neurons. J Neurophysiol *80*, 1-27.

Schultz, W. (2007). Multiple dopamine functions at different time courses. Annu Rev Neurosci *30*, 259-288.

Seamans, J.K., and Yang, C.R. (2004). The principal features and mechanisms of dopamine modulation in the prefrontal cortex. Prog Neurobiol *74*, 1-58.

Shi, S.Q., Bichell, T.J., Ihrie, R.A., and Johnson, C.H. (2015). Ube3a imprinting impairs circadian robustness in Angelman syndrome models. Curr Biol *25*, 537-545.

Sidorov, M.S., Krueger, D.D., Taylor, M., Gisin, E., Osterweil, E.K., and Bear, M.F. (2014). Extinction of an instrumental response: a cognitive behavioral assay in Fmr1 knockout mice. Genes Brain Behav.

Sparta, D.R., Hovelso, N., Mason, A.O., Kantak, P.A., Ung, R.L., Decot, H.K., and Stuber, G.D. (2014). Activation of prefrontal cortical parvalbumin interneurons facilitates extinction of reward-seeking behavior. J Neurosci *34*, 3699-3705.

Sparta, D.R., Stamatakis, A.M., Phillips, J.L., Hovelso, N., van Zessen, R., and Stuber, G.D. (2012). Construction of implantable optical fibers for long-term optogenetic manipulation of neural circuits. Nat Protoc *7*, 12-23.

Stamatakis, A.M., Jennings, J.H., Ung, R.L., Blair, G.A., Weinberg, R.J., Neve, R.L., Boyce, F., Mattis, J., Ramakrishnan, C., Deisseroth, K.*, et al.* (2013). A unique population of ventral tegmental area neurons inhibits the lateral habenula to promote reward. Neuron *80*, 1039-1053.

Stamatakis, A.M., and Stuber, G.D. (2012). Activation of lateral habenula inputs to the ventral midbrain promotes behavioral avoidance. Nat Neurosci *15*, 1105-1107.

Stuber, G.D., Hnasko, T.S., Britt, J.P., Edwards, R.H., and Bonci, A. (2010). Dopaminergic terminals in the nucleus accumbens but not the dorsal striatum corelease glutamate. J Neurosci *30*, 8229-8233.

Surmeier, D.J., Ding, J., Day, M., Wang, Z., and Shen, W. (2007). D1 and D2 dopamine-receptor modulation of striatal glutamatergic signaling in striatal medium spiny neurons. Trends Neurosci *30*, 228-235.

Talis, A.L., Huibregtse, J.M., and Howley, P.M. (1998). The role of E6AP in the regulation of p53 protein levels in human papillomavirus (HPV)-positive and HPV-negative cells. J Biol Chem *273*, 6439-6445.

Tritsch, N.X., Ding, J.B., and Sabatini, B.L. (2012). Dopaminergic neurons inhibit striatal output through non-canonical release of GABA. Nature *490*, 262-266.

Tritsch, N.X., Oh, W.J., Gu, C., and Sabatini, B.L. (2014). Midbrain dopamine neurons sustain inhibitory transmission using plasma membrane uptake of GABA, not synthesis. Elife *3*, e01936.

Tsai, H.C., Zhang, F., Adamantidis, A., Stuber, G.D., Bonci, A., de Lecea, L., and Deisseroth, K. (2009). Phasic firing in dopaminergic neurons is sufficient for behavioral conditioning. Science *324*, 1080-1084.

Tye, K.M., Mirzabekov, J.J., Warden, M.R., Ferenczi, E.A., Tsai, H.C., Finkelstein, J., Kim, S.Y., Adhikari, A., Thompson, K.R., Andalman, A.S.*, et al.* (2013). Dopamine neurons modulate neural encoding and expression of depression-related behaviour. Nature *493*, 537-541.

Wallace, M.L., Burette, A.C., Weinberg, R.J., and Philpot, B.D. (2012). Maternal loss of Ube3a produces an excitatory/inhibitory imbalance through neuron type-specific synaptic defects. Neuron *74*, 793-800.

Walsh, J.J., and Han, M.H. (2014). The heterogeneity of ventral tegmental area neurons: Projection functions in a mood-related context. Neuroscience *282C*, 101-108.

Williams, C.A., Beaudet, A.L., Clayton-Smith, J., Knoll, J.H., Kyllerman, M., Laan, L.A., Magenis, R.E., Moncla, A., Schinzel, A.A., Summers, J.A.*, et al.* (2006). Angelman syndrome 2005: updated consensus for diagnostic criteria. Am J Med Genet A *140*, 413-418.

Wise, R.A. (1978). Catecholamine theories of reward: a critical review. Brain Res *152*, 215-247.

Wise, R.A., and Rompre, P.P. (1989). Brain dopamine and reward. Annu Rev Psychol *40*, 191-225.

Yamaguchi, T., Sheen, W., and Morales, M. (2007). Glutamatergic neurons are present in the rat ventral tegmental area. Eur J Neurosci *25*, 106-118.

Yamamoto, Y., Huibregtse, J.M., and Howley, P.M. (1997). The human E6-AP gene (UBE3A) encodes three potential protein isoforms generated by differential splicing. Genomics *41*, 263-266.

Yashiro, K., Riday, T.T., Condon, K.H., Roberts, A.C., Bernardo, D.R., Prakash, R., Weinberg, R.J., Ehlers, M.D., and Philpot, B.D. (2009). Ube3a is required for experience-dependent maturation of the neocortex. Nat Neurosci *12*, 777-783.

Yim, C.Y., and Mogenson, G.J. (1980). Electrophysiological studies of neurons in the ventral tegmental area of Tsai. Brain Res *181*, 301-313.

Zhang, S., Qi, J., Li, X., Wang, H.L., Britt, J.P., Hoffman, A.F., Bonci, A., Lupica, C.R., and Morales, M. (2015). Dopaminergic and glutamatergic microdomains in a subset of rodent mesoaccumbens axons. Nat Neurosci *18*, 386-392.